



Shahrood University of
Technology



Iranian Society of
Mining Engineering
(IRSM)

Simulation of Crack Propagation Mechanism in Porous Media using Modified linear Element Displacement Discontinuity Method

Mohammadhosein Dehghani Firoozabadi¹, Mohammad Fatehi Marji^{1*}, Abolfazl abdollahipour², Alireza Yarahmadi Bafghi¹, and Yousef Mirzaeian¹

1. Department of Mining and Metallurgical Engineering, Faculty of Engineering, Yazd University, Yazd, Iran.

2. School of Mining Engineering, College of Engineering, University of Tehran, Tehran, Iran.

Article Info

Received 2 September 2022

Received in Revised form 25
September 2022

Accepted 30 September 2022

Published online 30 September
2022

[DOI:10.22044/jme.2022.12246.2223](https://doi.org/10.22044/jme.2022.12246.2223)

Keywords

Displacement discontinuity
method

Higher-order elements

Poroelastic

Fundamental solutions

Crack propagation

Abstract

In this work, an effective methodology is introduced for simulation of the crack propagation in linear poroelastic media. The presence of pores and saturated cracks that can be accompanied by fluid flow makes the use of poroelastic media inevitable. In this work, involvement of the time parameter in crack propagation is of particular importance. The order of doing the work is such that first, derives the fundamental solutions of a poroelastic higher order displacement discontinuity method (PHODDM). Then will be provided a numerical formulation and implementation for PHODDM in a code named linear element poroelastic DDM (LEP-DDM). Analytical solutions use different times to check the correctness and validity of the proposed solution and the newly developed code. The numerical results show a good agreement and coordination with the analytical results in time zero and 5000 seconds. The code is able to pursue crack-propagation in time and space. This topic is introduced and shown in an example.

1. Introduction

Among the numerical methods, the boundary element method (BEM) is particularly used in the field of linear elastic fracture mechanics (LEFM). This method is divided into two categories of direct and indirect

. The direct method can directly obtain the unknown boundary parameters (stresses and displacements) based on the specified boundary conditions. Thus it is known as a direct integration technique. In the indirect method, the solution is first performed for the singularities that satisfy the specified boundary conditions. The unknown parameters are then obtained indirectly through the standard numerical techniques in terms of these singular solutions. In the boundary element-based methods, since the governing differential equations are solved exactly in the domain of the problem,

they lead to a high accuracy in the solutions. BEM performs discretization only at the boundaries, thus reducing the dimensionality of the problem. This manner results in a smaller system of equations that are very cost-effective, as it significantly reduces the data required for analysis, and also eliminates the need for re-meshing using BEM, and crack growth may be modeled by adding a new element to the previous mesh. One of the common forms based on the boundary element is the dual boundary element method (DBEM), which consists of two combinations of independent boundary integral equations. Numerous investigations have been carried out concerning the growth of cracks based on DBEM in the 2D [2-4] and 3D [5-7] conditions.

Corresponding author: mohammad.fatehi@gmail.com (M. Fatehi Marji).

Discontinuity Discontinuity Method (DDM) is one of the other methods based on boundary element that is widely used in solving linear elastic fracture mechanics (LFEM) problems. First, Crouch and Starfield defined the basic principles of this technique [8, 9]. In this method, stresses and displacements at a point are calculated according to the discontinuity of normal and shear displacement. Many scientific research works have presented how to use constant ordinary elements in DDM [10-12]. Indeed, the main advantage of using these elements is their simplicity; however, they cannot correctly predict the stresses and displacements in the field points adjacent to the boundaries. Moreover, the singularity variations $1/r^{0.5}$ and $r^{0.5}$ in the stresses and displacement equations cause the calculation precision at the vicinity of the crack tip severely decrease [13].

In this regard, linear [14, 15], quadratic [16 & 17], and cubic higher-order [18 & 19] elements have been utilized to conquer these problems and obtain more correct values of stresses and displacements along boundaries. Based on the strain gradient stretching theory, Exadaktylos *et al.* and also a new constant displacement discontinuity element have been stated. This new method substantially improves the accuracy of DDM without using higher-order and crack tip elements [20-22]. The increase in accuracy is achieved by high-order elements. However, this does not work well for crack tip singularities. Therefore, crack tip elements were introduced to remove the obstacles [23]. To significantly increase the accuracy of analysis in crack problems, ordinary and crack tip higher-order elements are used simultaneously. Yan *et al.* have introduced constant crack tip elements to utilize in DDM [24]; they developed the procedure of the fatigue crack growth in the structures having multiple cracks [25]. Li and co-workers have used a method composed with the constant element displacement discontinuity method and meshless procedures to grow the crack in the static and cyclic loading conditions [26].

Cracks are the main flow channels in sub-surface rocks. It is important to state that the issues of crack propagation and fracture in artificial environments such as concrete and glass can be investigated and analyzed [27, 28]. Variation in the fluid pressure induces matrix deformation and stress variation; matrix deformation, in turn, induces fluid volume variation and fluid pressure variation. Possible fracture propagation results in the variation of pore pressure and stress in the whole field. The variation in pore pressure and stress at any point affect the fracture and induce fracture deformation. This

makes rocks exhibit a strong coupling of mechanical and hydrological behavior. To study this coupled hydro-mechanical behavior, the poroelasticity theory has been developed. Problems such as hydraulic fracturing [29-33], in-situ stress measurement [34-36], and geo-thermal [37-40] occurs in sub-surface rocks that are mostly filled with discontinuities (such as fissures and faults) and pores. These discontinuities and pores can be saturated with water, air, oil, etc. These fluids can greatly affect the stress (i.e. effective stresses due to pore pressure effect) and displacement fields in a rock mass. Also pore fluid flow occurs due to the pore pressure gradient in the rock. The flow can also be in response to changes in macroscopic stresses caused by natural factors such as tectonic forces and artificial factors such as drilling wells [41]. In order to accurately model these coupled interactions, all of these couplings must be considered. DDM has been coupled with other numerical methods such as FDM and FEM to inquire poroelastic effects of fracture [42-44]. For instance, Ji used DDM to simulate crack-propagation in porous media, and coupled it with FDM to simulate fluid interaction. Yin *et al.* coupled DDM and FEM to propound poroelastic effects in reservoirs. Bobet and Yu have presented a closed form solution of the crack-tip stress field [45]. They showed that the stresses created during the drying of the medium were higher than the stresses around the crack tip under pressure in a saturated medium. During the last decades, many studies have focused on providing a mathematical formulation or analytical solution for the hydraulic fracture problem in a porous rock [46-54].

This study discusses the parameters of crack-propagation in a porous medium. Then the required fundamental solutions for the poroelastic HODDM are derived. After that, numerical formulation and implementation of the HODDM in a poroelastic rock are introduced. After verifying the linear element poroelastic displacement discontinuity method code named LEP-DDM, the crack propagation in a porous medium is shown with an example.

2. Definition of higher order displacement discontinuity

A displacement discontinuity element of length $2a$ along the x -axis is depicted in Figure 1 (a), which is characterized by a general displacement discontinuity distribution $u(\xi)$. Considering the u_x and u_y components of the general displacement discontinuity $u(\xi)$ to be constant and equal to D_x

and D_y , respectively, in the interval $(-a, +a)$ as depicted in Figure 1 (b), two displacement discontinuity element surfaces can be distinguished, one on the positive side of y and another one on the negative side y .

The displacement endures a constant change in value when passing from one side of the displacement discontinuity element to the other side which may be defined as:

$$D_x = u_x(x, 0^-) - u_x(x, 0^+) \tag{1}$$

$$D_y = u_y(x, 0^-) - u_y(x, 0^+)$$

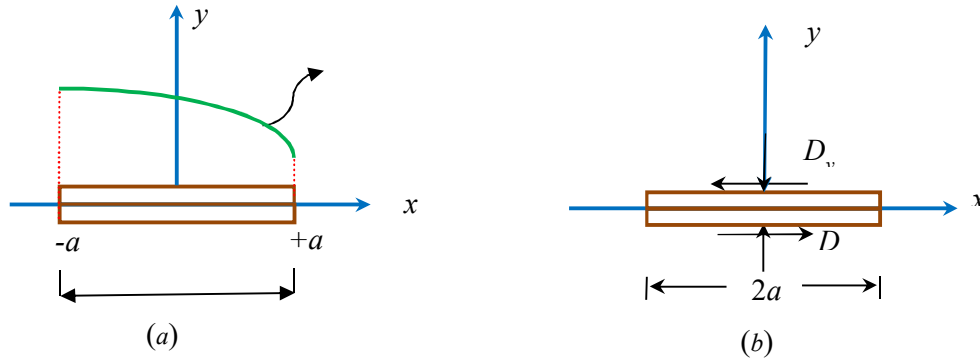


Figure 1. a) Distribution of $u(\xi)$ for general displacement discontinuity element. b) Constant element.

Figure 2.(a) depicts the linear displacement discontinuity distribution, which may be written in a general form as:

$$D_i(\xi) = N_1(\xi)(D_i)_1 + N_2(\xi)(D_i)_2 \tag{2}$$

$i = x, y$

where $(D_i)_1$ and $(D_i)_2$ are the linear displacement discontinuities, and

$$N_1(\xi) = -(\xi - a_2)/(a_1 + a_2) \tag{3}$$

$$N_2(\xi) = (\xi - a_1)/(a_1 + a_2)$$

are their linear collocation shape functions. It should be attentioned that a linear element has 2

The positive sign convention of D_x and D_y is depicted in Figure 1 (b), and demonstrates that when the two surfaces of the displacement discontinuity overlap, D_y is positive, which causes a physically impossible situation. This conceptual difficulty is overcome by considering that the element has a finite thickness in its undeformed state, which is small compared to its length but bigger than D_y [9]. The linear element displacement discontinuity formulation is based on the analytical integration of linear shape functions, straight-line displacement discontinuity elements.

nodes, which are the centers of the two elements within the path element [55].

3. SIF calculation and crack propagation parameters for poroelastic media

The Mode I and Mode II stress intensity factors K_I and K_{II} can be easily presumed based on the linear elastic fracture mechanics (LEFM) principles [56, 57]. A crack tip element of length $2a$ is considered after the SIFs with respect to the normal and shear displacement discontinuity (assuming plane strain condition) can be specified [55] as:

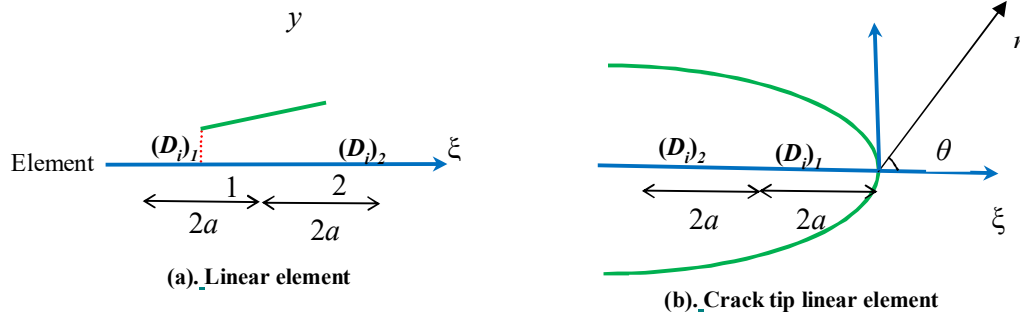


Figure 2. Location of nodes for higher order displacement discontinuity elements.

$$K_I = \frac{G}{4(1-\nu)} \sqrt{\frac{2\pi}{a}} D_y(a) \quad (4)$$

$$K_{II} = \frac{G}{4(1-\nu)} \sqrt{\frac{2\pi}{a}} D_x(a)$$

where G is the shear modulus, and ν is the Poisson's ratio of the brittle material. In poroelasticity, the discontinuities are time-dependent, so in this analysis, intensity factors (SIFs) Mode I and II are also time-dependent. K_I and K_{II} can be obtained by similar equations used in LEFM for DDM.

$$K_I(t) = \frac{G}{4(1-\nu)} \sqrt{\frac{2\pi}{a}} D_n(x, y, t) \quad (4)$$

$$K_{II}(t) = \frac{G}{4(1-\nu)} \sqrt{\frac{2\pi}{a}} D_s(x, y, t)$$

The initial condition of crack-propagation (for critical crack propagation) that is reaching a critical value (fracture toughness) can be satisfied by changing SIFs with time. The time dependence of SIFs indicates that crack propagation must have a certain rate in porous media, a quantity that is not present in elastic analysis. Therefore, by introducing time into the analysis, it should be considered that cracks take some time to grow to a certain length; therefore, a speed should be assigned to the crack propagation. In the proposed model, a time step Δt is considered. Crack-propagation in a porous medium requires the use of critical and sub-critical crack-propagation theories. Critical crack propagation takes place when Mode I SIF K_I and fracture toughness K_{IC} are equal. This propagation is inherently unstable, as once it starts, the stress value decreases to continue [58, 59]. The limiting speed or the maximum speed of critical crack propagation is equal to the speed of the Rayleigh wave [60]. Lithology, porosity, fluid content and temperature and stress field in rock formations change this speed. Sub-critical crack growth is often observed in rocks and minerals that experience prolonged or cyclic loading or high temperature. Cracks can propagate over a long period of time when K_I is less than K_{IC} [44]. This theory is implemented in this research work.

The power-law relationship between crack sub-critical velocity and SIF is written in the form of:

$$v = v_{max} \left(k_I / k_{IC} \right)^n \quad (6)$$

where V_{max} is a constant, and n is a sub-critical index

[44]. The speed may be chosen based on the nature of the crack-propagation being used (critical or subcritical propagation).

Maximum tangential stress criterion is used for evaluation of crack propagation and initiation angle [61]. In each time increment Δt , crack elements will grow a length of:

$$\Delta L = V \times \Delta t \quad (7)$$

When ΔL reaches a pre-determined growth increment length, a boundary element is added to that crack element to indicate a growth event.

4. Poroelastic

The theory of linear, isotropic poroelasticity was proposed by Biot for modeling the response of fluid-saturated porous solids [62], and was further extended by others [63, 64]. According to the original formula of Biot, the basic dynamic parameters of total stress σ_{ij} and pore pressure p along with their corresponding quantities, solid strain $e_{ij} = (u_{i,j} + u_{j,i})/2$ and change of fluid volume per unit reference ζ are considered here. A fixed set of parameters for linear isotropic theory are shear modulus G , drained and undrained Poisson ratios, which are, respectively, $\nu = (3K - 2G)/2(3K + G)$, $\nu_u = (3Ku - 2G)/2(3Ku + G)$ (drained and undrained bulk moduli K and Ku), Skempton's pore pressure coefficient S (ratio of induced pore pressure to variation of confined pressure in undrained conditions), and permeability coefficient $\kappa = k/\mu$ (where k is intrinsic permeability and μ fluid dynamic viscosity) [62]. The governing equations of linear isotropic poroelasticity consist of the following [62]:

• Constitutive equations:

$$\sigma_{ij} = 2G e_{ij} + \frac{2G\nu}{1-2\nu} \delta_{ij} e - \alpha \delta_{ij} p \quad (8)$$

$$p = -\frac{2GS(1+\nu_u)}{3(1-2\nu_u)} e + \frac{2GS^2(1-2\nu)(1+\nu_u)^2}{9(\nu_u-\nu)(1-2\nu_u)} \zeta \quad (9)$$

• Equilibrium equations

$$\sigma_{ij,j} = -F_i \quad (10)$$

• Darcy's law

$$q_i = -\kappa(p_{,i} - f_i) \quad (11)$$

• Continuity equation

$$\frac{\partial \zeta}{\partial t} + q_{i,i} = \gamma \tag{12}$$

where, in the above equations, $e = e_{ii}$ is the volumetric strain, $F_i = \rho g_i$ bulk body force (solid and fluid), g_i gravity component in i direction, n porosity, q_i specific discharge, ζ variation of fluid content, $\rho = (1-n)\rho_s + \phi\rho_f$ bulk density, ρ_s and ρ_f solid and fluid part densities respectively, $f_i = \rho_f g_i$ fluid body force, γ fluid injection rate from the fluid source, and α is the Biot coefficient of effective stress, defined as:

$$\alpha = \frac{3(\nu_u - \nu)}{S(1 - 2\nu)(1 + \nu_u)} \tag{13}$$

The foregoing can be combined to yield a set of field equations in terms of displacement and fluid content change. Combining Equations (8) to (10) yields an elasticity equation with a fluid coupling term:

$$G\nabla^2 u_i + \frac{G}{1 - 2\nu_u} e_{,i} - \frac{2GS(1 + \nu_u)}{3(1 - 2\nu_u)} \zeta_{,i} = -F_i \tag{14}$$

Combining Equations (9), (11), and (12), and also using Eq (14), produces the following diffusion equation:

$$\frac{\partial \zeta}{\partial t} - c\nabla^2 \zeta = \frac{kS(1 + \nu_u)}{3(1 - \nu_u)} F_{i,i} - kf_{i,i} + \gamma \tag{15}$$

where

$$C = \frac{2kS^2G(1 - \nu)(1 + \nu_u)^2}{9(1 - \nu_u)(\nu_u - \nu)} \tag{16}$$

is a generalized consolidation coefficient [64]. The above equations can be used to obtain the required solution for HODDM in porous rock.

5. Fundamental solutions of higher order displacement discontinuity method in poroelastic medium

Detournay, Cheng, and Abdollahipour have presented the poroelastic solution of point plane strain displacement discontinuity based on dislocation theory [65, 66] (see Appendix A). In Appendix A, the first displacement subscript indicates the displacement component, while the second subscript (and the last one in all parameters) is reserved for dislocation mode (1 for sliding mode, 2 for normal mode).

Poroelastic influence functions for HODDM can be obtained by distributing this solution over an element domain Γ_λ located on the local s -axis (Figure 3). For example, using the following integrals, it is possible to obtain the value of the stress in the local n direction caused by the discontinuity of the normal displacement.

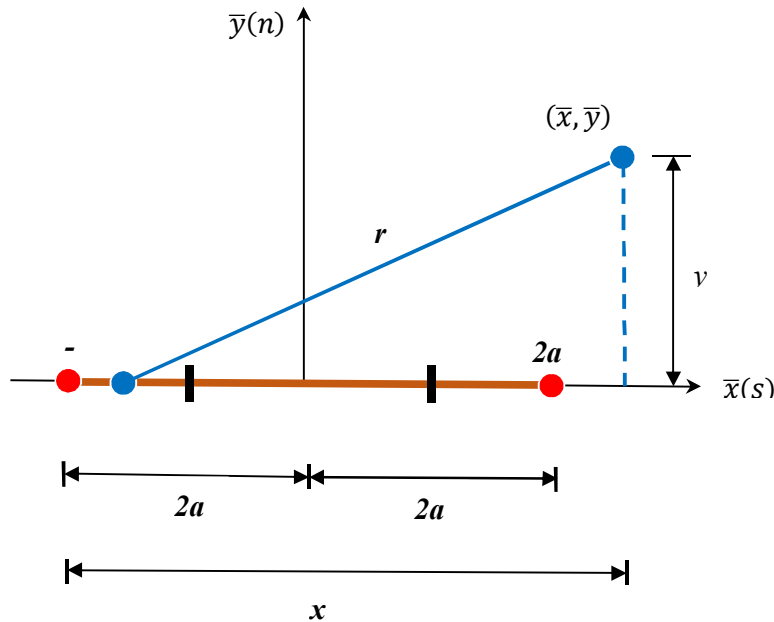


Figure 3. A higher order element in local coordinates.

$$p^j(\bar{x}, \bar{y}, t) = p^{dn}(\bar{x}, \bar{y}, t) \sum_{w=1}^2 N_w(D_n)_w + p^{ds}(\bar{x}, \bar{y}, t) \sum_{w=1}^2 N_w(D_s)_w + p^f(\bar{x}, \bar{y}, t) D_f^j \quad (19)$$

$$\begin{aligned} \sigma_{\bar{x}\bar{x}}^j(\bar{x}, \bar{y}, t) &= \sigma_{\bar{x}\bar{x}}^{dn}(\bar{x}, \bar{y}, t) \sum_{w=1}^2 N_w(D_n)_w + \sigma_{\bar{x}\bar{x}}^{ds}(\bar{x}, \bar{y}, t) \sum_{w=1}^2 N_w(D_s)_w + \sigma_{\bar{x}\bar{x}}^f(\bar{x}, \bar{y}, t) D_f^j \\ \sigma_{\bar{y}\bar{y}}^j(\bar{x}, \bar{y}, t) &= \sigma_{\bar{y}\bar{y}}^{dn}(\bar{x}, \bar{y}, t) \sum_{w=1}^2 N_w(D_n)_w + \sigma_{\bar{y}\bar{y}}^{ds}(\bar{x}, \bar{y}, t) \sum_{w=1}^2 N_w(D_s)_w + \sigma_{\bar{y}\bar{y}}^f(\bar{x}, \bar{y}, t) D_f^j \\ \sigma_{\bar{x}\bar{y}}^j(\bar{x}, \bar{y}, t) &= \sigma_{\bar{x}\bar{y}}^{dn}(\bar{x}, \bar{y}, t) \sum_{w=1}^2 N_w(D_n)_w + \sigma_{\bar{x}\bar{y}}^{ds}(\bar{x}, \bar{y}, t) \sum_{w=1}^2 N_w(D_s)_w + \sigma_{\bar{x}\bar{y}}^f(\bar{x}, \bar{y}, t) D_f^j \end{aligned} \quad (20)$$

where D_n , D_s , and D_f are discontinuities in normal and shear displacement and discontinuity in flux, respectively. The induced stresses in the j th element can be converted to the global coordinates using coordinate transformation equations. Pore pressure does not require coordinate transformation because it is a scalar value, and is invariant in all coordinate systems.

By converting Equations 19 and 20 to the local coordinate system of the i th element, the stresses induced in the i th element caused by the j th element are obtained.

Normal and shear stresses and pore pressure caused by fluid injection/production at a constant rate and linear shear and normal displacement discontinuities of the j element are created on the i th element are

$$\begin{aligned} \sigma_n^{ij} &= A_{ns} \sum_{w=1}^2 N_w(D_s)_w + A_{nn} \sum_{w=1}^2 N_w(D_n)_w + A_{nf} D_f^j \\ \sigma_s^{ij} &= A_{ss} \sum_{w=1}^2 N_w(D_s)_w + A_{sn} \sum_{w=1}^2 N_w(D_n)_w + A_{sf} D_f^j \\ p^{ij} &= A_{fs} \sum_{w=1}^2 N_w(D_s)_w + A_{fn} \sum_{w=1}^2 N_w(D_n)_w + A_{ff} D_f^j \end{aligned} \quad (21)$$

$$\begin{aligned} A_{ns}^{ij}(x, y, t) &= \cos^2 \gamma \sigma_{\bar{x}\bar{x}}^{ds}(\bar{x}, \bar{y}, t) \sum_{w=1}^2 N_w(D_s)_w + \sin 2\gamma \sigma_{\bar{x}\bar{y}}^{ds}(\bar{x}, \bar{y}, t) \sum_{w=1}^2 N_w(D_s)_w \\ &+ \sin^2 \gamma \sigma_{\bar{y}\bar{y}}^{ds}(\bar{x}, \bar{y}, t) \sum_{w=1}^2 N_w(D_s)_w A_{nn}(\bar{x}, \bar{y}, t) \\ &= \cos^2 \gamma \sigma_{\bar{x}\bar{x}}^{dn}(\bar{x}, \bar{y}, t) \sum_{w=1}^2 N_w(D_n)_w + \sin 2\gamma \sigma_{\bar{x}\bar{y}}^{dn}(\bar{x}, \bar{y}, t) \sum_{w=1}^2 N_w(D_n)_w \\ &+ \sin^2 \gamma \sigma_{\bar{y}\bar{y}}^{dn}(\bar{x}, \bar{y}, t) \sum_{w=1}^2 N_w(D_n)_w \\ A_{nf}^{ij}(x, y, t) &= \cos^2 \gamma \sigma_{\bar{x}\bar{x}}^f(\bar{x}, \bar{y}, t) + \sin 2\gamma \sigma_{\bar{x}\bar{y}}^f(\bar{x}, \bar{y}, t) + \sin^2 \gamma \sigma_{\bar{y}\bar{y}}^f(\bar{x}, \bar{y}, t) \\ A_{ss}^{ij}(x, y, t) &= \sin \gamma \cos \gamma \left(\sigma_{\bar{x}\bar{x}}^{ds}(\bar{x}, \bar{y}, t) \sum_{w=1}^2 N_w(D_s)_w - \sigma_{\bar{y}\bar{y}}^{ds}(\bar{x}, \bar{y}, t) \sum_{w=1}^2 N_w(D_s)_w \right) \\ &- \left(\cos^2 \gamma - \sin^2 \gamma \right) \sigma_{\bar{x}\bar{y}}^{ds}(\bar{x}, \bar{y}, t) \sum_{w=1}^2 N_w(D_s)_w \end{aligned} \quad (22)$$

$$\begin{aligned}
 A_{Sn}^{ij}(x, y, t) &= \sin \gamma \cos \gamma \left(\sigma_{\bar{x}\bar{x}}^{dn} \left(x, y, t \right) \sum_{w=1}^2 N_w (D_n)_w - \sigma_{\bar{y}\bar{y}}^{dn} \left(x, y, t \right) \sum_{w=1}^2 N_w (D_n)_w \right) \\
 &\quad - \left(\cos^2 \gamma - \sin^2 \gamma \right) \sigma_{\bar{x}\bar{y}}^{dn} \left(x, y, t \right) \sum_{w=1}^2 N_w (D_n)_w \\
 A_{Sf}^{ij}(x, y, t) &= \sin \gamma \cos \gamma \left(\sigma_{\bar{x}\bar{x}}^f \left(x, y, t \right) - \sigma_{\bar{y}\bar{y}}^f \left(x, y, t \right) \right) - \left(\cos^2 \gamma - \sin^2 \gamma \right) \sigma_{\bar{x}\bar{y}}^f \left(x, y, t \right) \\
 A_{fs}^{ij}(x, y, t) &= p^{ds} \left(x, y, t \right) \sum_{w=1}^2 N_w (D_s)_w \\
 A_{fn}^{ij}(x, y, t) &= p^{dn} \left(x, y, t \right) \sum_{w=1}^2 N_w (D_n)_w \\
 A_{ff}^{ij}(x, y, t) &= p^f \left(x, y, t \right)
 \end{aligned} \tag{22}$$

In the problem, A_{nn}^{ij} is the boundary stress influence coefficients. The coefficient A_{nn}^{ij} , for instance, gives the actual normal stress at the quarter point and three quarter point of the i th element (σ_n^i) due to a linear normal displacement discontinuity applied to the j th element at time t , while $\sigma_{\bar{x}\bar{x}}^{dn} \left(x, y, t \right)$ are the influence functions including both the time-independent and time-dependent parts. For example, $\sigma_{\bar{x}\bar{y}}^{ds} \left(x, y, t \right)$ presents local stress $\sigma_{\bar{x}\bar{y}}$ at the quarter point and three quarter point of the i th element due to a sheara displacement discontinuity at the j th element in time t , and $\gamma = \theta_i - \theta_j$ is the angle between element i and j and:

$$\begin{aligned}
 x &= (x_i - x_j) \cos \theta_j + (y_i - y_j) \sin \theta_j \\
 y &= -(x_i - x_j) \sin \theta_j + (y_i - y_j) \cos \theta_j
 \end{aligned} \tag{23}$$

For the time-dependent part of shear and normal discontinuities, D_s and D_n and flux discontinuity D_f , a time marching method is used. This method decomposes time into N fixed steps, and then uses superposition to calculate each step change at the time it occurs. Except for the first time step, the constant step source does not start at time zero ($t = 0$). Therefore, In order to be able to use the fundamental solution and influence coefficients, a time shift is necessary. For example, consider the linear amounts $N_w(\Delta D_n)_w(x_j, y_j, \tau_\omega)$, $N_w(\Delta D_s)_w(x_j, y_j, \tau_\omega)$, and $\Delta D_f(x_j, y_j, \tau_\omega)$, which belong to the j th element at the time τ_ω are added; it results in the induced stresses and pore pressure in Equation 24 on the i th element at time t .

$$\begin{aligned}
 \sigma_n^i &= \sum_{j=1}^M A_{ns}^{ij}(t - \tau_\omega) \sum_{w=1}^2 N_w^{j\omega} (\Delta D_s)_w + \sum_{j=1}^M A_{nn}^{ij}(t - \tau_\omega) \sum_{w=1}^2 N_w^{j\omega} (\Delta D_n)_w + \sum_{j=1}^M A_{nq}^{ij}(t - \tau_\omega) \Delta D_f^{j\omega} \\
 \sigma_s^i &= \sum_{j=1}^M A_{ss}^{ij}(t - \tau_\omega) \sum_{w=1}^2 N_w^{j\omega} (\Delta D_s)_w + \sum_{j=1}^M A_{sn}^{ij}(t - \tau_\omega) \sum_{w=1}^2 N_w^{j\omega} (\Delta D_n)_w + \sum_{j=1}^M A_{sf}^{ij}(t - \tau_\omega) \Delta D_f^{j\omega} \\
 p^i &= \sum_{j=1}^M A_{fs}^{ij}(t - \tau_\omega) \sum_{w=1}^2 N_w^{j\omega} (\Delta D_s)_w + \sum_{j=1}^M A_{fn}^{ij}(t - \tau_\omega) \sum_{w=1}^2 N_w^{j\omega} (\Delta D_n)_w + \sum_{j=1}^M A_{ff}^{ij}(t - \tau_\omega) \Delta D_f^{j\omega}
 \end{aligned} \tag{24}$$

where $N_w(\Delta D_s)_w$, $N_w(\Delta D_n)_w$, and ΔD_f are shear and normal displacement discontinuities increments and flux discontinuity increment of the

j th element at time τ_ω and the number of elements is displayed with M . Finally, by summing the influence functions of all time steps ω , the total

stresses and pore pressure induced on the *i*th element at time *t* are obtained.

A set of five integral equations must be solved to determine displacement discontinuity and flux discontinuity. The dependence of normal and shear stresses and pore pressure on the history of displacement discontinuities and flux discontinuities determines how to choose these integrals

6. Expression of numerical formulation of poroelastic HODDM

$$\begin{aligned}
 \sigma_n^i(t) &= \sum_{\omega=0}^h \sum_{j=1}^M A_{ns}(t - \tau_\omega) \sum_{w=1}^2 N_w(\Delta D_s)_w^{j\omega} + \sum_{\omega=0}^h \sum_{j=1}^M A_{nn}(t - \tau_\omega) \sum_{w=1}^2 N_w(\Delta D_n)_w^{j\omega} + \sum_{\omega=0}^h \sum_{j=1}^M A_{nf}(t - \tau_\omega) \Delta D_f^{j\omega} \\
 \sigma_s^i(t) &= \sum_{\omega=0}^h \sum_{j=1}^M A_{ss}(t - \tau_\omega) \sum_{w=1}^2 N_w(\Delta D_s)_w^{j\omega} + \sum_{\omega=0}^h \sum_{j=1}^M A_{sn}(t - \tau_\omega) \sum_{w=1}^2 N_w(\Delta D_n)_w^{j\omega} + \sum_{\omega=0}^h \sum_{j=1}^M A_{sf}(t - \tau_\omega) \Delta D_f^{j\omega} \quad (25) \\
 \dot{p}^i(t) &= \sum_{\omega=0}^h \sum_{j=1}^M A_{fs}(t - \tau_\omega) \sum_{w=1}^2 N_w(\Delta D_s)_w^{j\omega} + \sum_{\omega=0}^h \sum_{j=1}^M A_{fn}(t - \tau_\omega) \sum_{w=1}^2 N_w(\Delta D_n)_w^{j\omega} + \sum_{\omega=0}^h \sum_{j=1}^M A_{ff}(t - \tau_\omega) \Delta D_f^{j\omega}
 \end{aligned}$$

$$\begin{aligned}
 \sigma_s(x, t) &= l_{i2}(x)l_{j1}(x) \left[\int_0^t \int_\Gamma l_{ik}(\zeta)l_{jl}(\zeta)\sigma_{kl}^{ds}(x, \zeta, t - \tau)N_1(D_s)_1(\zeta, \tau)d\Gamma(\zeta)d\tau \right. \\
 &+ \int_0^t \int_\Gamma l_{ik}(\zeta)l_{jl}(\zeta)\sigma_{kl}^{ds}(x, \zeta, t - \tau)N_2(D_s)_2(\zeta, \tau)d\Gamma(\zeta)d\tau \\
 &+ \int_0^t \int_\Gamma l_{ik}(\zeta)l_{jl}(\zeta)\sigma_{kl}^{dn}(x, \zeta, t - \tau)N_1(D_n)_1(\zeta, \tau)d\Gamma(\zeta)d\tau \quad (26) \\
 &+ \int_0^t \int_\Gamma l_{ik}(\zeta)l_{jl}(\zeta)\sigma_{kl}^{dn}(x, \zeta, t - \tau)N_2(D_n)_2(\zeta, \tau)d\Gamma(\zeta)d\tau \\
 &\left. + \int_0^t \int_\Gamma l_{ik}(\zeta)l_{jl}(\zeta)\sigma_{kl}^{df}(x, \zeta, t - \tau)D_f(\zeta, \tau)d\Gamma(\zeta)d\tau \right]
 \end{aligned}$$

$$\begin{aligned}
 \sigma_n(x, t) &= l_{i2}(x)l_{j2}(x) \left[\int_0^t \int_\Gamma l_{ik}(\zeta)l_{jl}(\zeta)\sigma_{kl}^{ds}(x, \zeta, t - \tau)N_1(D_s)_1(\zeta, \tau)d\Gamma(\zeta)d\tau \right. \\
 &+ \int_0^t \int_\Gamma l_{ik}(\zeta)l_{jl}(\zeta)\sigma_{kl}^{ds}(x, \zeta, t - \tau)N_2(D_s)_2(\zeta, \tau)d\Gamma(\zeta)d\tau \\
 &+ \int_0^t \int_\Gamma l_{ik}(\zeta)l_{jl}(\zeta)\sigma_{kl}^{dn}(x, \zeta, t - \tau)N_1(D_n)_1(\zeta, \tau)d\Gamma(\zeta)d\tau \quad (27) \\
 &+ \int_0^t \int_\Gamma l_{ik}(\zeta)l_{jl}(\zeta)\sigma_{kl}^{dn}(x, \zeta, t - \tau)N_2(D_n)_2(\zeta, \tau)d\Gamma(\zeta)d\tau \\
 &\left. + \int_0^t \int_\Gamma l_{ik}(\zeta)l_{jl}(\zeta)\sigma_{kl}^{df}(x, \zeta, t - \tau)D_f(\zeta, \tau)d\Gamma(\zeta)d\tau \right]
 \end{aligned}$$

$$p(x, t) = \int_0^t \int_\Gamma P_s(x, \zeta, t - \tau)N_1(D_s)_1(\zeta, \tau)d\Gamma(\zeta)d\tau + \int_0^t \int_\Gamma P_s(x, \zeta, t - \tau)N_2(D_s)_2(\zeta, \tau)d\Gamma(\zeta)d\tau \quad (28)$$

$$\begin{aligned}
 & + \int_0^t \int_{\Gamma} P_n(x, \zeta, t - \tau) N_1(D_n)_1(\zeta, \tau) d\Gamma(\zeta) d\tau + \int_0^t \int_{\Gamma} P_n(x, \zeta, t - \tau) N_2(D_n)_2(\zeta, \tau) d\Gamma(\zeta) d\tau \\
 & + \int_0^t \int_{\Gamma} P_f(x, \zeta, t - \tau) D_f(\zeta, \tau) d\Gamma(\zeta) d\tau
 \end{aligned}$$

and Γ is element locus. The subscripts i, j, k , and l vary from 1 to 2, and Einstein's sum convention is considered on them. A global coordinate system (x, y) and a local coordinate (\bar{x}_1, \bar{x}_2) where its axes

\bar{x}_1 and \bar{x}_2 equivalent, respectively, with the tangential (s) and normal (n) directions of the element are assumed here (see Figure 5).

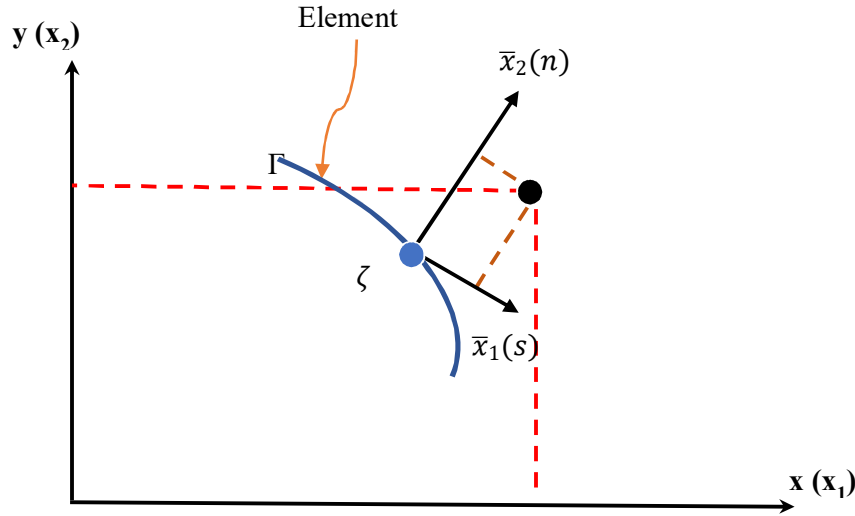


Figure 5. Local and global coordinate systems.

The coordinate conversion between the global and local systems is performed using Equation (29).

$$\bar{x}_j = l_{ij}(x_i - o_i) \tag{29}$$

where \bar{x}_j ($j = 1, 2$ or n, s) is local coordinate system, l_{ij} is the rotational tensor, x_i ($i = 1, 2$) are global coordinate system, and o_i is the origin of the local system in global coordinates. Influence functions $\sigma_{kl}^{dn}(x, \eta, t - \tau)$ represent stress components expressed in local coordinate system at point x and time t due to a unit impulse normal displacement discontinuity located at η and occurring time τ . σ_{kl}^{ds} and σ_{kl}^{df} have similar meanings. P_s, P_n , and P_f are influence functions for discontinuities $N_w(D_s)_w, N_w(D_n)_w$ and D_f .

7. Numerical implementation of linear element poroelastic DDM (LEP-DDM)

The system of equations (26) to (28) can be solved numerically using the following method.

- Initially, the geometry is separated into m elements and the time interval from 0 to t into h time steps.
- Then discontinuities D_s, D_n , and D_f are considered over each element $\lambda \in [1, m]$ and time step $\omega \in [1, h]$ using appropriate shape functions in time and space.
- Using numerical integration, the Equations (26) to (28), a linear system of equations is generated.
- At the end of the first stage, the system of equations is solved, and leads to the determination of discontinuities at the one-quarter point and three-quarter point of each element (linear elements are used).
- The time march of the solution (D_s, D_n , and D_f) is found at the end of each time step until the last time step is reached.

Also some simplifications and assumptions are considered.

- As mentioned, linear elements are used.
- Collocation points are the quarter point and three quarter point of each element.

- Discontinuities are linear over each element.
- Discontinuities change linearly with time.
- The time steps Δt are considered constant.

Equations (26) to (28) can be expressed as a double summation of integrals over time and space using the above method and assumptions. For instance, Equation (27) at points x^{β_1} and x^{β_2} and time t may be written as Equation (30).

$$\begin{aligned} \sigma_n^h(x^\lambda, t) = & l_{i_2}^{\beta_1} l_{j_2}^{\beta_1} \sum_{\omega=1}^h \sum_{\lambda=1}^m l_{i_k}^\lambda l_{j_l}^\lambda \times \\ & \left\{ \int_0^{\Delta t} \left[N_1(D_n^\lambda)_1((\omega - 1)\Delta t + \tau) \int_{\Gamma^\lambda} \sigma_{kl}^{dn}(x^{\beta_1}, \zeta, (h - \omega + 1)\Delta t - \tau) d\Gamma(\zeta) \right] dt + \right. \\ & \int_0^{\Delta t} \left[N_1(D_s^\lambda)_1((\omega - 1)\Delta t + \tau) \int_{\Gamma^\lambda} \sigma_{kl}^{ds}(x^{\beta_1}, \zeta, (h - \omega + 1)\Delta t - \tau) d\Gamma(\zeta) \right] dt + \\ & \left. \int_0^{\Delta t} \left[D_f^\lambda((\omega - 1)\Delta t + \tau) \int_{\Gamma^\lambda} \sigma_{kl}^{df}(x^{\beta_1}, \zeta, (h - \omega + 1)\Delta t - \tau) d\Gamma(\zeta) \right] dt \right\} + l_{i_2}^{\beta_2} l_{j_1}^{\beta_2} \sum_{\omega=1}^h \sum_{\lambda=1}^m l_{i_k}^\lambda l_{j_l}^\lambda \times \quad (30) \\ & \left\{ \int_0^{\Delta t} \left[N_2(D_n^\lambda)_2((\omega - 1)\Delta t + \tau) \int_{\Gamma^\lambda} \sigma_{kl}^{dn}(x^{\beta_2}, \zeta, (h - \omega + 1)\Delta t - \tau) d\Gamma(\zeta) \right] dt + \right. \\ & \int_0^{\Delta t} \left[N_2(D_s^\lambda)_2((\omega - 1)\Delta t + \tau) \int_{\Gamma^\lambda} \sigma_{kl}^{ds}(x^{\beta_2}, \zeta, (h - \omega + 1)\Delta t - \tau) d\Gamma(\zeta) \right] dt + \\ & \left. \int_0^{\Delta t} \left[D_f^\lambda((\omega - 1)\Delta t + \tau) \int_{\Gamma^\lambda} \sigma_{kl}^{df}(x^{\beta_2}, \zeta, (h - \omega + 1)\Delta t - \tau) d\Gamma(\zeta) \right] dt \right\} \end{aligned}$$

$$\sigma_{kl}^{dn,\lambda}(x^\lambda; t) = \int_{\Gamma^\lambda} N_1(D_n^\lambda)_1 \sigma_{kl}^{dn}(x^{\beta_1}, \zeta, t) d\Gamma(\zeta) + \int_{\Gamma^\lambda} N_2(D_n^\lambda)_2 \sigma_{kl}^{dn}(x^{\beta_2}, \zeta, t) d\Gamma(\zeta) \quad (31)$$

The above equation is the spatial integral of Equation (30).

The exact solution of these space integrals in a local coordinate system (on element domain Γ^λ , which is located on the local axes s) were provided and presented in the Appendix B. The time integrals are calculated numerically.

The interpolation of discontinuities between the values at the beginning and end of each time step is done linearly.

Substituting Equations (32), (33) and (31) in Equation (30) and ordering according to the discontinuities results in the following linear equation based on unknowns $N_w(D_s)_{w,\lambda,h}$, $N_w(D_n)_{w,\lambda,h}$,

and $D_f^{\lambda,h}$, where $\sigma_n^h(x^\lambda, t)$ is known boundary condition in time h . The values of $N_w(D_s)_{w,\lambda,\omega}$, $N_w(D_n)_{w,\lambda,\omega}$, and $D_f^{\lambda,\omega}$ are known for time step $\omega \in [0, h - 1]$ from the earlier solutions. Therefore, they become clear on the right-hand side

of Equation (34). As mentioned earlier, the superposition of these known parameters from the earlier time steps updates the boundary conditions (the right-hand of Equation (34) for the new equation to be solved. The unknown and known coefficients of A and B, respectively, are written as follow:

$$N_1(D_n^\lambda)_1((\omega - 1)\Delta t + \tau) = \frac{1}{\Delta t} [(\Delta t - \tau)N_1(D_n^{\lambda,\omega-1})_1 + \tau N_1(D_n^{\lambda,\omega})_1] \quad (32)$$

$$N_2(D_n^\lambda)_2((\omega - 1)\Delta t + \tau) = \frac{1}{\Delta t} [(\Delta t - \tau)N_2(D_n^{\lambda,\omega-1})_2 + \tau N_2(D_n^{\lambda,\omega})_2] \quad (33)$$

$$0 \leq \tau \leq \Delta t$$

$$\sum_{\lambda=1}^m A_{ns}^\lambda \sum_{w=1}^2 N_w(D_s)^{\lambda,h} + \sum_{\lambda=1}^m A_{nn}^\lambda \sum_{w=1}^2 N_w(D_n)^{\lambda,h} + \sum_{\lambda=1}^m A_{nf}^\lambda D_f^{\lambda,h}$$

$$= \sigma_n^h(x^\lambda, t) - \sum_{\omega=0}^{h-1} \sum_{\lambda=1}^m B_{ns}^{\lambda,\omega} \sum_{w=1}^2 N_w(D_s)^{\lambda,\omega} - \sum_{\omega=0}^{h-1} \sum_{\lambda=1}^m B_{nn}^{\lambda,\omega} \sum_{w=1}^2 N_w(D_n)^{\lambda,\omega} - \sum_{\omega=0}^{h-1} \sum_{\lambda=1}^m B_{nf}^{\lambda,\omega} D_f^{\lambda,\omega}$$

(34)

$$A_{nn}^\lambda = l_{i2}^{\beta_1} l_{j2}^{\beta_1} l_{ik}^\lambda l_{jl}^\lambda \int_0^{\Delta t} \frac{\tau}{\Delta t} N_1(D_n^\lambda)_1 \sigma_{kl}^{n,\lambda}(x^{\beta_1}; \Delta t - \tau) d\tau +$$

$$l_{i2}^{\beta_2} l_{j2}^{\beta_2} l_{ik}^\lambda l_{jl}^\lambda \int_0^{\Delta t} \frac{\tau}{\Delta t} N_2(D_n^\lambda)_2 \sigma_{kl}^{n,\lambda}(x^{\beta_2}; \Delta t - \tau) d\tau$$

$$B_{nn}^{\lambda,\omega} = l_{i2}^{\beta_1} l_{j2}^{\beta_1} l_{ik}^\lambda l_{jl}^\lambda \int_0^{\Delta t} \left[\frac{\Delta t - \tau}{\Delta t} N_1(D_n^\lambda)_1 \sigma_{kl}^{n,\lambda}(x^{\beta_1}; (h - \omega)\Delta t - \tau) + \frac{\tau}{\Delta t} N_1(D_n^\lambda)_1 S_{n,kl}^\lambda(x^{\beta_1}; (h - \omega + 1)\Delta t - \tau) \right] d\tau$$

(35)

$$+ l_{i2}^{\beta_2} l_{j2}^{\beta_2} l_{ik}^\lambda l_{jl}^\lambda \int_0^{\Delta t} \left[\frac{\Delta t - \tau}{\Delta t} N_2(D_n^\lambda)_2 \sigma_{kl}^{n,\lambda}(x^{\beta_2}; (h - \omega)\Delta t - \tau) + \frac{\tau}{\Delta t} N_2(D_n^\lambda)_2 S_{n,kl}^\lambda(x^{\beta_2}; (h - \omega + 1)\Delta t - \tau) \right]$$

$d\tau, \omega \neq 0$

$$B_{nn}^{\lambda,0} = l_{i2}^{\beta_1} l_{j2}^{\beta_1} l_{ik}^\lambda l_{jl}^\lambda \int_0^{\Delta t} \frac{\Delta t - \tau}{\Delta t} N_1(D_n^\lambda)_1 \sigma_{kl}^{n,\lambda}(x^{\beta_1}; h\Delta t - \tau) d\tau + l_{i2}^{\beta_2} l_{j2}^{\beta_2} l_{ik}^\lambda l_{jl}^\lambda \int_0^{\Delta t} \frac{\Delta t - \tau}{\Delta t} N_2(D_n^\lambda)_2 \sigma_{kl}^{n,\lambda}(x^{\beta_2}; h\Delta t - \tau) d\tau$$

Similar coefficients may be derived for shear and flux.

The Gauss-Legendre quadrature method with seven points is used for numerical integration required for time integrals. Because of Dirac delta function in time kernels, coefficient A is separated into two parts before integration, where $(A_{nn}^\lambda)^0$ is

the time-independent part, and can be obtained from Equation (37) and $\Delta(A_{nn}^\lambda)$ is the time-dependent part of the unknown coefficient A and can be obtained from Equation

Coefficient B is also separated into two parts.

$$A_{nn}^\lambda = (A_{nn}^\lambda)^0 + \Delta(A_{nn}^\lambda) \tag{36}$$

$$(A_{nn}^\lambda)^0 = l_{i2}^{\beta_1} l_{j2}^{\beta_1} l_{ik}^\lambda l_{jl}^\lambda N_1(D_n^\lambda)_1 (\sigma_{kl}^{dn,\lambda})^0(x^{\beta_1}) + l_{i2}^{\beta_2} l_{j2}^{\beta_2} l_{ik}^\lambda l_{jl}^\lambda N_2(D_n^\lambda)_2 (\sigma_{kl}^{dn,\lambda})^0(x^{\beta_2}) \tag{37}$$

$$\Delta(A_{nn}^\lambda) = l_{i2}^{\beta_1} l_{j2}^{\beta_1} l_{ik}^\lambda l_{jl}^\lambda \int_0^{\Delta t} \frac{\tau}{\Delta t} N_1(D_n^\lambda)_1 \Delta(\sigma_{kl}^{dn,\lambda})(x^{\beta_1}; \Delta t - \tau) d\tau$$

(38)

$$+ l_{i2}^{\beta_2} l_{j2}^{\beta_2} l_{ik}^\lambda l_{jl}^\lambda \int_0^{\Delta t} \frac{\tau}{\Delta t} N_2(D_n^\lambda)_2 \Delta(\sigma_{kl}^{dn,\lambda})(x^{\beta_2}; \Delta t - \tau) d\tau$$

$$B_{nn}^\lambda = (B_{nn}^{\lambda,\omega})^1 + (B_{nn}^{\lambda,\omega})^2 \tag{39}$$

$$(B_{nn}^{\lambda,\omega})^1 = l_{ik}^\lambda l_{jl}^\lambda l_{i2}^{\beta_1} l_{j2}^{\beta_1} \int_0^{\Delta t} \left[\frac{\Delta t - \tau}{\Delta t} N_1(D_n^\lambda)_1 \Delta(\sigma_{kl}^{dn,\lambda})(x^{\beta_1}; (h - \omega)\Delta t - \tau) \right] d\tau$$

(40)

$$+ l_{ik}^\lambda l_{jl}^\lambda l_{i2}^{\beta_2} l_{j2}^{\beta_2} \int_0^{\Delta t} \left[\frac{\Delta t - \tau}{\Delta t} N_2(D_n^\lambda)_2 \Delta(\sigma_{kl}^{dn,\lambda})(x^{\beta_2}; (h - \omega)\Delta t - \tau) \right] d\tau$$

$$\begin{aligned}
 (B_{nn}^{\lambda, \omega})^2 &= l_{ik}^\lambda l_{jl}^\lambda l_{i_2^1}^{\beta_1} l_{j_2^1}^{\beta_1} \int_0^{\Delta t} \left[\frac{\tau}{\Delta t} N_1(D_n^\lambda)_1 \Delta(\sigma_{kl}^{dn, \lambda})(x^{\beta_1}; (h - \omega + 1)\Delta t - \tau) \right] d\tau \\
 &+ l_{ik}^\lambda l_{jl}^\lambda l_{i_2^1}^{\beta_2} l_{j_2^1}^{\beta_2} \int_0^{\Delta t} \left[\frac{\tau}{\Delta t} N_2(D_n^\lambda)_2 \Delta(\sigma_{kl}^{dn, \lambda})(x^{\beta_2}; (h - \omega + 1)\Delta t - \tau) \right] d\tau
 \end{aligned}
 \tag{41}$$

Coefficients $(A_{nn}^\lambda)^0$ and $\Delta(A_{nn}^\lambda)$ are independent from h , and are determined only once. In each time step, only coefficients $(B_{nn}^{\lambda, 0})^1$ and $(B_{nn}^{\lambda, 0})^2$ are evaluated; the other coefficients are determined at earlier time steps.

The discretized Equations (30) are collocated at the quarter point and three quarter point of the elements for boundary condition σ_n . Similar coefficients can be achieved for σ_s and p . Eventually, for M boundary elements can create $3M$ linear equations for $3M$ unknown discontinuities (D_n, D_s, D_f) at time $t = h \Delta t$. We consider that the section related to normal and shear discontinuities each has two unknown discontinuities. The matrix notation for the system of linear equations may be expressed as follows:

$$AD^h = -\left(\sum_{\omega=0}^{h-1} B^n D^n - \sigma^h \right) \tag{42}$$

The error function $erf(x)$ is expressed in the time-dependent part of the influence functions in the Appendix B. This is a special function (non-

elementary), which is expressed in probability, statistics, and partial differential equations describing diffusion [67, 68]. The following estimation is used for this function with maximum error of 1.2×10^{-7} [69]. The estimation is valid over the complete range of values.

$$erf(x) = \begin{cases} -(1 - \tau) & \text{for } x \geq 0 \\ -(1 + \tau) & \text{for } x < 0 \end{cases} \tag{43}$$

8. Validation of developed poroelastic code LEP-DDM

In the following, crack opening displacements in different situations are presented to study the performance and accuracy of the proposed code. These problems have been previously presented analytically. A suddenly pressurized crack in an infinite body is used in order to investigate the linear element poroelastic DDM (LEP-DDM) code developed here. Consider a thin crack under constant internal pressure p with a length of $2L$ (see Figure 6).

$$\begin{aligned}
 \tau &= t \times \exp(-x^2 - 1.26551223 + 1.00002378t + 0.37409196t^2 + 0.09678418t^3 \\
 &- 0.18628806t^4 + 0.27886807t^5 - 1.13520398t^6 + 1.48751587t^7 - 0.82215223t^8 + 0.17087277t^9)
 \end{aligned}
 \tag{44}$$

$$t = \frac{1}{-(-1 - 0.5|x|)} \tag{45}$$

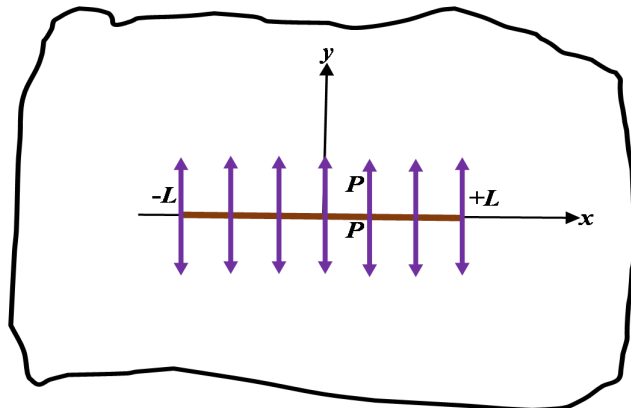


Figure 6. A suddenly pressurized crack.

The exact amount of relative normal displacement of crack surfaces (crack opening displacement) COD in an elastic medium in Equation (46) can be calculated [70].

$$COD = \frac{2p(1 - \nu)}{G} \sqrt{L^2 - x^2} \tag{46}$$

where $-L \leq x \leq L$.

In the first time steps in a porous medium, it shows undrained behavior because the fluid inside the pores cannot escape (elastic response with undrained specification), and around the crack, the pore pressure increases. Therefore, analytic's solutions must be compared with the results of the first time step, which represents an elastic behavior. A crack with length $2L = 1$ m from $x = -0.5$ m to $x = +0.5$ m and properties of Table 1 with no farfield stress and 25 MPa internal pressure with $\Delta t = 0.05$ s is used for validation.

Figure 7 shows crack opening displacement (COD) in the direction of x -axis using the

analytical and numerical methods (LEP-DDM code) and 20 linear elements in a short time and a long time. As it can be seen, the numerical results are in good agreement and coordination with the analytical results. The values of the numerical results are slightly over-predicted. The pore pressure will dissipate after a long period of internal pressure applied to the crack and a drained behavior (elastic response with drained specification) appears. Figure 7 shows the results of the numerical model after 5000 s and analytical models using drained Poisson ratio.

Table 1. Parameters of model.

Skempton's coefficient (S)	0.90
UndrainedPoisson ratio (ν_u)	0.29
Drained Poisson ratio (ν)	0.10
Permeability (κ) (mdarcy)	1
Biot's coefficient (α)	0.67
Generalizedconsolidationcoefficient(c)(m2/s)	0.003
Shear modulus(G) (GPa)	14

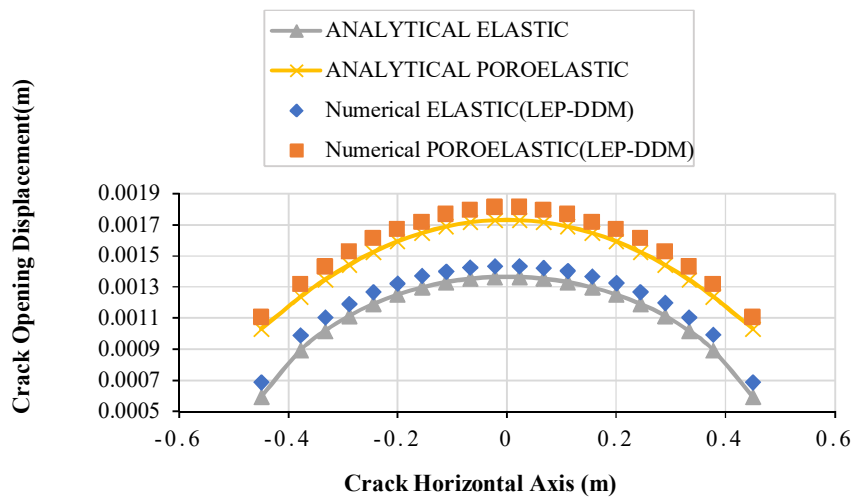


Figure 7. Numerical and analytical results of COD in long time and short time.

Another example is used to illustrate crack propagation in poroelastic media. It is important to note that once a new element is added, the coefficients $(A_{nn}^\lambda)^0$ and $\Delta(A_{nn}^\lambda)$ of the previous time step are no longer valid, and they must be re-assessed because each new element adds 3 new unknowns D_n , D_s , and D_f (section related to normal and shear discontinuities each has two unknown discontinuities) to the set of linear equations. The following fourteen steps describe the procedure for performing crack-propagation analysis in LEP-DDM.

1. Start

2. We define geometry
3. We solve the linear elastic system at zero time
4. We update the boundary conditions
5. We solve the linear elastic system in the new time step
6. We calculate the stress intensity factor
7. We check whether crack propagation occurs or no
8. If the answer is negative, we go back to step 4; otherwise, we go to step 9
9. Have we reached the length described?

10. If the answer is negative, we go to step 7; otherwise, we go to step 11
11. A new element is added
12. Solving the same time step for the new unknown achieve
13. We return to step 9
14. End

To demonstrate crack-propagation in a poroelasticity, two parallel cracks in a porous rock under far-field compressive stresses $\sigma_x = 57 \text{ MPa}$, $\sigma_y = 47 \text{ MPa}$ with the initial length and the same distance of 50 cm have been used. An internal pressure of 60 MPa is applied to the cracks. Sub-critical crack propagation is used. In geological formations, the velocity of crack propagation varies based on temperature and grain size from 10^{10} to 10^{-16} m/s in sub-critical propagation [71].

Crack propagation velocity of 10^{-11} m/s along with sub-critical index $n = 25$ were used for this demonstration. Figure 8 depicts crack-propagation in a poroelastic rock after 100, 200, 400, and 4000 time steps. The cracks start to diverge from each other at first and over time; they align with the maximum far-field stress.

To show the time-dependent SIF, a pressurized crack (by applying internal pressure 60 MPa) with similar properties to the previous example was modeled. Figure 9 depicts the variations of Mode I SIF with time for 500 s. As it can be seen, SIF is high at the beginning and gradually reduces as time passes; the reducing trend is much faster after 400 s. SIF would reach 0 if the model were run indefinitely (since no far-field stress or pore pressure was considered) and the internal pressure of the crack would completely dissipate.

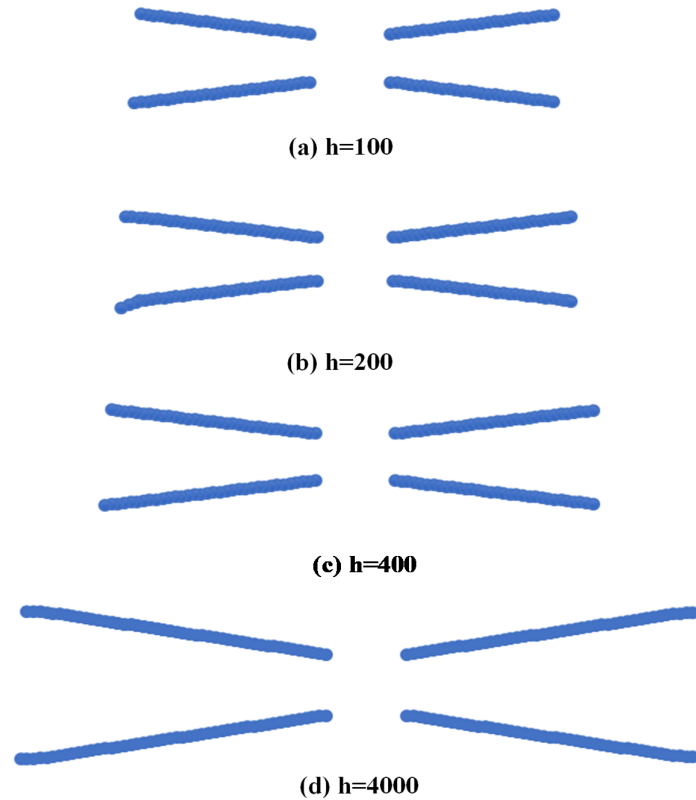


Figure 8. Crack-propagation in a poroelastic rock after various time steps.

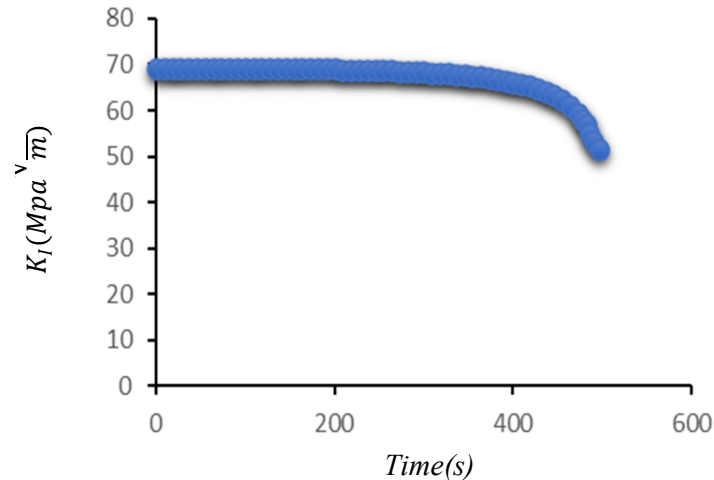


Figure 9. Variations of normal SIF with time for a pressurized crack by applying internal pressure $P = 60$ Mpa.

9. Conclusions

The present study introduced linear higher-order elements, and newly developed a higher-order numerical code (LEP-DDM) using linear displacement discontinuity in poroelastic medium. Since the fundamental solutions in the displacement discontinuity method (DDM) involve a displacement jump, this method is suitable for problem involving fractures and discontinuities. However, the original DDM and its higher-order extensions are all restricted to elastic problems. In geo-mechanics, many situations such as hydraulic fracturing, in-situ stress measurement, and geo-thermal occur in a poroelastic media.

Since the porous media are affected by the deformation-diffusion behavior, it is necessary to use the theory of poroelasticity. The possibility of developing boundary element methods for porous media can be achieved when the fundamental solutions of poroelastic media are presented. In order to derive the fundamental solutions for the porous higher order displacement discontinuity, the fundamental solutions of the higher order displacement discontinuity of the impulse point and the source were used. The fundamental solution creates the influence function in the final DDM formulation. To use these functions, the boundary field is divided into several boundary sub-elements.

Field and geometric variables are interpolated by piecewise polynomials.

After numerical formulation and implementation for the poroelastic HO-DDM in LEP-DDM code was provided. At this stage, the equations are numerically integrated and the solution of the linear form including discrete variables in space is

produced. Integral equations have a time part and the time integral is solved.

The accuracy and validity of the new formulation and numerical implementation were proved using the analytical solutions. The response at $t = 0$ and long duration is obtained using the undrained and drained Poisson's ratio for analytical solutions after applying internal pressure. These results showed good agreement and coordination with numerical results at first time step and a long time ($t = 5000$ s) later. Crack-propagation, which enables the code to pursue crack propagation issues in time and space, is described in 14 steps. In the following, an example for crack propagation simulation in a poroelastic rock was provided and crack propagation was showed. At the end, the time dependency of SIFs in a poroelastic medium was illustrated by mentioning another example. Since the crack propagation velocity must be determined for this part. As a result, poroelastic problems depend on time.

References

- [1]. Crouch .S.L, and Starfield. A.M. (1983). Boundary Element Methods in Solid Mechanics: With Applications in Rock Mechanics and Geological Engineering. Allen & Unwin.
- [2]. Portela. A, Aliabadi M.H., and Rooke DP. (1992).The dual boundary element method: effective implementation for crack problems. Int J Numer Methods Eng ;33 (6): 1269–87.
- [3]. de Matos .P.F.P., Moreira .P.M.G.P, Portela .A, and de Castro .P.M.S.T. (2004).Dual boundary element analysis of cracked plates:post-processing implementation of the singularity subtraction technique Comput Struct ;82 (17-19):1443-9.

- [4]. Santana .E. and Portela. A. (2016). Dual boundary element analysis of fatigue crack growth, interaction and linkup. *EngAnal Bound Elem* ;64:176–95. <https://doi.org/10.1016/j.enganabound.2015.12.002>.
- [5]. dell'Erba. D.N. and Aliabadi .M.H. (2000). Three-dimensional thermo-mechanical fatigue crack growth using BEM. *Int J Fatigue* ;22:261–73. [https://doi.org/10.1016/S0142-1123\(00\)00011-6](https://doi.org/10.1016/S0142-1123(00)00011-6).
- [6]. Cisilino. A.P. and Aliabadi .M.H. (2004). Dual boundary element assessment of three-dimensional fatigue crack growth. *Eng Anal BoundElem*;28:1157–73. <https://doi.org/10.1016/j.enganabound.2004.01.005>.
- [7]. Wang. P.B. and Yao .Z.H. (2006). Fast multipole DBEM analysis of fatigue crack growth. *ComputMech* ;38(3):22333. <https://doi.org/10.1007/s00466-005-0743-9>.
- [8]. Crouch. S.L.(1976). Engineering U of MD of C and M, Program NSF (U. S). RA to NN. Analysis of Stresses and Displacements Around Underground Excavations.
- [9]. Crouch. S.L. (1976). Solution of plane elasticity problems by the displacement discontinuity method. I. Infinite body solution. *Int J Numer Methods Eng*;10 (2): 301–343.
- [10]. Chaoxi. L, Suaris. W.(1991). Hadamard's principle for displacement discontinuity modeling of cracks. *Eng Fract Mech* ;39:141–5. [https://doi.org/10.1016/0013-7944\(91\)90029-Z](https://doi.org/10.1016/0013-7944(91)90029-Z).
- [11]. Fatehi Marji. M. (2011). On the crack propagation mechanism of brittle rocks under various loading conditions. <https://doi.org/10.5593/sgem2011/s02.131>.
- [12]. Haeri Hadi, Shahriar Kouros, Marji Mohammad Fatehi, and Moarefvand Parviz. (2014). Experimental and numerical study of crack propagation and coalescence in precracked rock-like disks. *Int J Rock Mech Min Sci* ;67:20–8.
- [13]. Fatehi Marji. M. (2014). Rock fracture mechanics with displacement discontinuity method. *Ger L Lambert Acad Publ*.
- [14]. Crawford. A.M. and Curran .J.H. (1982). Higher-order functional variation displacement discontinuity elements. *Int J Rock Mech Min Sci Geomech Abstr* ;19:143–8.
- [15]. Napier. J.A.L and Malan .D.F. (1997). A viscoplastic discontinuum model of time-dependent fracture and seismicity effects in brittle rock. *Int J Rock Mech Min Sci* ;34 (7): 1075–89.
- [16]. Marji Mohammad Fatehi. (2015). Simulation of crack coalescence mechanism underneath single and double disc cutters by higher order displacement discontinuity method. *J Cent South Univ* ;22 (3):1045–54.
- [17]. Abdollahipour. A. and Fatehi Marji. M. (2020). A thermo-hydronechanical displacement discontinuity method to model fractures in high-pressure, high-temperature environments. *RenewEnergy*;153:1488–503.
- [18]. Marji. M.F. (1996). Modeling of cracks in rock fragmentation with a higher order displacement discontinuity method. Ankara, Turkey: Middle East Technical University.
- [19]. Abdollahipour Abolfazl, Marji Mohammad Fatehi, Bafghi Alireza Yarahmadi, and Gholamnejad Javad. (2016). On the accuracy of higher order displacement discontinuity method (HODDM) in the solution of linear elastic fracture mechanics problems. *J Cent South Univ*. 23 (11): 2941–50.
- [20]. Exadaktylos. G and Xiroudakis. G.(2010). The G2 constant displacement discontinuity method–Part I: Solution of plane crack problems. *Int J Solids Struct* ;47 (18-19): 2568–77.
- [21]. Exadaktylos. G and Xiroudakis. G.(2010). The G2 constant displacement discontinuity method–Part II: Solution of half-plane crack problems. *Int J Solids Struct* ; 47 (18-19): 2578–90.
- [22]. Exadaktylos. George and Xiroudakis. George.(2010). A G2 constant displacement discontinuity element for analysis of crack problems. *Comput Mech* ;45 (4): 245–61.
- [23]. Marji. M.F, Hosseini-Nasab. H, and Kohsary. A.H.(2007). A new cubic element formulation of the displacement discontinuity method using three special crack tip elements for crack analysis. *JP J Solids Struct* ;1:61–91.
- [24]. Yan. X.(2005). An efficient and accurate numerical method of stress intensity factors calculation of a branched crack. *J Appl Mech*;72:330–40.
- [25]. Yan. Xiangqiao.(2006). Multiple crack fatigue growth modeling by displacement discontinuity method with crack-tip elements. *Appl Math Model* ;30 (6): 489–508.
- [26]. Li. J, Sladek J, Sladek. V, and Wen PH. (2020). Hybrid meshless displacement discontinuity method (MDDM) in fracture mechanics: static and dynamic. *Eur J Mech* ;83: 104023. <https://doi.org/10.1016/j.euromechsol.2020.10402>.
- [27]. Haeri. Hadi.(2015). Experimental crack analyses of concrete-like CSCBD specimens using a higher order DDM, *Journal of computers and concrete*, Volume 16, Issue 6, Pages 881-896.
- [28]. D. Fakhri; M. Hosseini, and M. Mahdikhani. (2022). Effect of Glass and Polypropylene Hybrid Fibers on Mode I, Mode II, and Mixed-Mode Fracture Toughness of Concrete Containing Micro-Silica and Limestone Powder, *Journal of Mining and Environment*, Volume 13, Issue 2, Pages 559-577.

- [29]. Naredran .V.M and Cleary .M.P.(1989). Analysis of growth and interaction of multiple hydraulic fractures. Reserv. Stimul. Symp., San Francisco.
- [30]. Adachi .J.I and Detournay. E. (2008). Plane strain propagation of a hydraulic fracture in a permeable rock. *Engng Fract Mech* ;75:4666–94. mech.2008.04.006.
- [31]. Ito. T.(2008). Effect of pore pressure gradient on fracture initiation in fluid saturated porous media: *Rock. Eng Fract Mech* ;75:1753–62. doi:10.1016/j.engfracmech.2007.03.028.
- [32]. Huang, J, Griffiths. D.V.V, and Wong. S. (2012). Initiation pressure, location and orientation of hydraulic fracture. *Int J Rock Mech Min Sci* ;49:59–67.2011.11.014.
- [33]. Yu. W., Luo. Z., Javadpour. F., and Varavei. A., Sepehrnoori. K.(2013). Sensitivity analysis of hydraulic fracture geometry in shale gas reservoirs. *J Pet Sci Eng*2014;113:1–7. doi:10.1016/j.petrol.2013.12.005.
- [34]. Bush DD and Barton N.(1989). Application of small-scale hydraulic fracturing for stress measurements in bedded salt. *Int J Rock Mech Min Sci Geomech Abstr* ; 26:629–35.
- [35]. Schmitt. D.R and Zoback .M.D.(1989). Poroelastic effects in the determination of the maximum horizontal principal stress in hydraulic fracturing tests—A proposed breakdown equation employing a modified effective stress relation for tensile failure. *Int J Rock Mech Min Sci Geomech Abstr* ; 26:499–506.
- [36]. Abdollahipour. A, Fatehi Marji. M, and Yarahmadi-Bafghi. A.R. (2013). A fracture mechanics concept of in-situ stress measurement by hydraulic fracturing test. 6th Int. Symp. In-situ Rock Stress, Sendai, Japan: ISRM.
- [37]. Legarth. B, Huenges E, and Zimmermann. G. (2005). Hydraulic fracturing in a sedimentary geothermal reservoir: Results and implications. *Int J Rock Mech Min Sci* ;42:1028–1041.
- [38]. Reinicke. A, Zimmermann. G .(2010). Hydraulic stimulation of a deep sandstone reservoir to develop an enhanced geothermal system:laboratory and field experiments. *Geothermics*39:70–77. doi:10.1016/j.geothermics.2009.12.003.
- [39]. Davis. R. and Carter. L.(2013). Fracking Doesn't Cause Significant Earthquakes. Durham Univesity.
- [40]. Hofmann. H, Babadagli. T, and Zimmermann. G. Hot water generation for oil sands processing from enhanced geothermal systems: Process simulation for different hydraulic fracturing scenarios. *Appl Energy* 113:524–547.
- [41]. Jaeger J, Cook N, and Zimmerman R. (2009). *Fundamentals of rock mechanics*. Wiley, New York.
- [42]. Boonei. T.J, Ingrffea. A.R, Roegiers. J-C .(1991). Simulation of hydraulic fracture propagation in poroelastic rock with application to stress measurement techniques. *Int J Rock Mech Min Sci Geomech abstr* 28:1–14.
- [43]. Yin. S, Dusseault. M.B, and Rothenburg L. (2007). Analytical and numerical analysis of pressure drawdown in a poroelastic reservoir with complete overburden effect considered. *Adv Water Resour* 30:1160–1167.
- [44]. Ji. L. (2013). Geomechanical aspects of fracture growth in a poroelastic, chemically reactive environment. The University of Texas at Austin .
- [45]. Bobet A and Yu H. (2015). Stress field near the tip of a crack in a poroelastic transversely anisotropic saturated rock. *Eng Fract Mech* 141:1–18.
- [46]. Greetesma J and de Klerk F. (1969). A rapid method of predicting width and extent of hydraulic induced fractures. *J Pet Tech* 21:1571–1581.
- [47]. Detournay E. (2004). Propagation regimes of fluid-driven fractures in impermeable rocks. *Int J Geomech* 4:35–45.
- [48]. Mitchell S, Kuske R, and Peirce. A. (2006). An asymptotic framework for finite hydraulic fractures including leak-off. *SIAM J Appl Math* 67:364–386.
- [49]. Garagash. D. (2007). Plane-strain propagation of a fluid-driven fracture during injection and shut-in: asymptotics of large toughness. *Engng Fract Mech* 74:456–481.
- [50]. Mitchell. S, Kuske. R, and Peirce. A .(2007). An asymptotic framework for the analysis of hydraulic fractures: the impermeable case. *J Appl Mech Trans ASME* 74:365–372.
- [51]. Hu. J and Garagash. D (2010). Plane-strain propagation of a fluid driven crack in a permeable rock with fracture toughness. *J Eng Mech ASCE* 136:1152–1166.
- [52]. Lobao. M, Eve. R, Owen. D.R.J et al. (2010). Modelling of hydrofracture flow in porous media. *Engng Comput* 27:129–154. doi:10.1108/02644401011008568.
- [53]. Behnia. M, Goshtasbi. K, Fatehi Marji. M, and Golshani. A.(2012). On the crack propagation modeling of hydraulic fracturing by a hybridized displacement discontinuity/ boundary collocation method. *J Min Environ*;2.
- [54]. Darvish. H, Nouri-Taleghani. M, Shokrollahi. A, and Tatar. A (2015). Geo-mechanical modeling and selection of suitable layer for hydraulic fracturing operation in an oil reservoir (south west of Iran). *J African Earth Sci*; 111:409–20.
- [55]. Shou K. J. and Crouch S. L. (1995). 'A Higher Order Displacement Discontinuity Method for Analysis of Crack Problems'; *Int. J. Rock Mech. Min. Sci. and Geomech. Abstr*, 32, pp. 49-55.

[56]. Sanford. R.J (2003). Principles of fracture mechanics. Prentice Hall, Upper Saddle River.

[57]. Fatehi Marji. M, Hosseini Nasab. H, and Kohsary. A.H (2006). On the uses of special crack tip elements in numerical rock fracture mechanics. Int J Solids. Struct43:1669–1692.doi:10.1016/j.ijsolstr.2005.04.042.

[58]. Lawn. R and Wilshaw. R (1975). Review indentation fracture: principles and applications. J Mater Sci 10:1049–1081.

[59]. Pollard. D.D and Aydin. A (1988). Progress in understanding jointing over the past century. Geol Soc Am Bull 100:1181–1204.

[60]. Morozov. V.A and Savenkov. G.G. (2013). Limiting velocity of crack propagation in dynamically fractured materials. J Appl Mech Tech Phys 54:142–147.

[61]. Erdogan. F, Sih. G.C. (1963). On the crack extension in plates under plate loading and transverse shear. J Basic Eng 85:519–27

[62]. Biot. M.A. (1941). General theory of three-dimensional consolidation. J Appl Phys 12:155–164.

[63]. Verruijt. A. (1969). Elastic storage in aquifers. Flow through porous media. Academic Press, New York, pp 331–376.

[64]. Rice. J.R and Cleary. M.P. (1976). Some basic stress diffusion solutions for fluid saturated elastic porous media with compressible constituents. Rev Geophys 14:227–241.

[65]. Detournay. E and Cheng. A. (1987). Poroelastic solution of a plane strain point displacement discontinuity.

[66]. Abdollahipour .A. (2015). Crack propagation mechanism in hydraulic fracturing procedure in oil reservoirs. University of Yazd, Yazd.

[67]. Andrews L.C. (1985). Special functions for engineers and applied mathematicians. Macmillan, London.

[68]. Greene. W.H (2003). Econometric analysis. Pearson Education, Gurgaon.

[69]. Teukolsky. S.A, Vetterling WT, and Flannery .B.P. (1996). Numeical recipes in Fortran 77 and Fortran 90. Cambridge University Press, Cambridge.

[70]. Sneddon. I.N (1951). Fourier transforms. McGraw-Hill Book Company, New York.

[71]. Atkinson. B.K (1984). Subcritical crack growth in geological minerals. J Geophys Res 89:4077–4114.

Appendix A

$$(u_{ij})^0 = -\frac{1}{4\pi(1-\nu_u)} H(t) \frac{1}{r} [(1-2\nu_u)(\delta_{il}r_{,2} + \delta_{iz}r_{,j} - \delta_{jz}r_{,l}) + 2r_{,i}r_{,j}r_{,2}] \quad (A_1)$$

$$\Delta u_{ij}^{dc} = -\frac{\nu_u - \nu}{4\pi(1-\nu_u)(1-\nu)} \frac{1}{r} [(2r_{,i}r_{,j}r_{,2} - \delta_{jz}r_{,i})e^{-\xi^2 + (\delta_{iz}r_{,j} + \delta_{jz}r_{,i} - \delta_{ij}r_{,2} - 4r_{,i}r_{,j}r_{,2})\xi^{-2}}(1-e^{-\xi^2})] \quad (A_2)$$

$$(\sigma_{ijk})^0 = -\frac{G}{2\pi(1-\nu_u)} \delta(t) \frac{1}{r^2} [8r_{,i}r_{,j}r_{,k}r_{,2} - 2(\delta_{kz}r_{,i}r_{,j} + \delta_{ij}r_{,k}r_{,2}) - (\delta_{ik}\delta_{jz} + \delta_{jk}\delta_{iz} - \delta_{ij}\delta_{kz})] \quad (A_3)$$

$$\begin{aligned} \Delta \sigma_{ijk} = & -\frac{2Gc(\nu_u - \nu)}{\pi(1-\nu)(1-\nu_u)} \frac{1}{r^4} ([24r_{,i}r_{,j}r_{,k}r_{,2} - 12(\delta_{ij}r_{,k}r_{,2} + \delta_{kz}r_{,i}r_{,j}) \\ & - 3(\delta_{ik}\delta_{jz} + \delta_{jk}\delta_{iz} - 3\delta_{ij}\delta_{kz})][1 - (1 + \xi^2)e^{-\xi^2}] \\ & - [12r_{,i}r_{,j}r_{,k}r_{,2} - 6(\delta_{kz}r_{,i}r_{,j} + \delta_{ij}r_{,k}r_{,2}) - 2\delta_{ik}\delta_{jz} - 2\delta_{jk}\delta_{iz} + 4\delta_{ij}\delta_{kz}]\xi^4 e^{-\xi^2} \\ & - [4r_{,i}r_{,j}r_{,k}r_{,2} - 4(\delta_{ij}r_{,k}r_{,2} + \delta_{kz}r_{,i}r_{,j}) + 4\delta_{ij}\delta_{kz}]\xi^6 e^{-\xi^2} \end{aligned} \quad (A_4)$$

$$(p_i)^0 = \frac{BG(1+\nu_u)}{3\pi(1-\nu_u)} \delta(t) \frac{1}{r^2} (\delta_{iz} - 2r_{,i}r_{,2}) \quad (A_5)$$

$$p_i = \frac{4BGc(1+\nu_u)}{3\pi(1-\nu_u)} \frac{1}{r^4} (\delta_{iz}\xi^4 e^{-\xi^2} + 2(r_{,i}r_{,2} - c\delta_{iz})\xi^6 e^{-\xi^2}) \quad (A_6)$$

$$(q_{ij})^0 = \frac{3c(\nu_u - \nu)}{\pi B(1-\nu)(1+\nu_u)} \delta(t) \frac{1}{r^3} (\delta_{iz}r_{,j} + \delta_{jz}r_{,i} + \delta_{ij}r_{,2} - 4r_{,i}r_{,j}r_{,2}) \quad (A_7)$$

$$\Delta q_{ij} = -\frac{6c^2(v_u - v)}{\pi B(1 - v)(1 + v_u)} \frac{1}{r^5} \left[2(\delta_{i2}r_{,j} + \delta_{ij}r_{,2} - 3\delta_{j2}r_{,i})\xi^6 e^{-\xi^2} + 4(\delta_{j2}r_{,i} - r_{,i}r_{,j}r_{,2})\xi^8 e^{-\xi^2} \right] \quad (\text{A}_8)$$

Appendix B

Time-independent part of influence functions

$$(\sigma_{yy}^{ds,\lambda})^0 = \frac{G}{4\pi(1 - v_u)} \left[\left(\frac{y(y^2 - (x - 2a_1)^2)}{((x - 2a_1)^2 + y^2)^2} - \frac{y(y^2 - (x + 2a_1)^2)}{((x + 2a_1)^2 + y^2)^2} \right) + \left(\frac{y(y^2 - (x - 2a_2)^2)}{((x - 2a_2)^2 + y^2)^2} - \frac{y(y^2 - (x + 2a_2)^2)}{((x + 2a_2)^2 + y^2)^2} \right) \right] \quad (\text{B}_1)$$

$$(\sigma_{xx}^{ds,\lambda})^0 = \frac{G}{4\pi(1 - v_u)} \left[\left(\frac{y(3(x - 2a_1)^2 + y^2)}{((x - 2a_1)^2 + y^2)^2} - \frac{y(3(x + 2a_1)^2 + y^2)}{((x + 2a_1)^2 + y^2)^2} \right) + \left(\frac{y(3(x - 2a_2)^2 + y^2)}{((x - 2a_2)^2 + y^2)^2} - \frac{y(3(x + 2a_2)^2 + y^2)}{((x + 2a_2)^2 + y^2)^2} \right) \right] \quad (\text{B}_2)$$

$$(\sigma_{yx}^{ds,\lambda})^0 = \frac{G}{4\pi(1 - v_u)} \left[\left(\frac{(x - 2a_1)(y^2 - (x - 2a_1)^2)}{((x - 2a_1)^2 + y^2)^2} - \frac{(x + 2a_1)(y^2 - (x + 2a_1)^2)}{((x + 2a_1)^2 + y^2)^2} \right) + \left(\frac{(x - 2a_2)(y^2 - (x - 2a_2)^2)}{((x - 2a_2)^2 + y^2)^2} - \frac{(x + 2a_2)(y^2 - (x + 2a_2)^2)}{((x + 2a_2)^2 + y^2)^2} \right) \right] \quad (\text{B}_3)$$

$$(\sigma_{xx}^{dn,\lambda})^0 = \frac{G}{4\pi(1 - v_u)} \left[\left(\frac{(x - 2a_1)(y^2 - (x - 2a_1)^2)}{((x - 2a_1)^2 + y^2)^2} - \frac{(x + 2a_1)(y^2 - (x + 2a_1)^2)}{((x + 2a_1)^2 + y^2)^2} \right) + \left(\frac{(x - 2a_2)(y^2 - (x - 2a_2)^2)}{((x - 2a_2)^2 + y^2)^2} - \frac{(x + 2a_2)(y^2 - (x + 2a_2)^2)}{((x + 2a_2)^2 + y^2)^2} \right) \right] \quad (\text{B}_4)$$

$$(\sigma_{yy}^{dn,\lambda})^0 = -\frac{G}{4\pi(1-\nu_u)} \left[\left(\frac{(x-2a_1)((x-2a_1)^2+3y^2)}{((x-2a_1)^2+y^2)^2} - \frac{(x+2a_1)((x+2a_1)^2+3y^2)}{((x+2a_1)^2+y^2)^2} \right) + \left(\frac{(x-2a_2)((x-2a_2)^2+3y^2)}{((x-2a_2)^2+y^2)^2} - \frac{(x+2a_2)((x+2a_2)^2+3y^2)}{((x+2a_2)^2+y^2)^2} \right) \right] \tag{B5}$$

$$(\sigma_{yx}^{dn,\lambda})^0 = \frac{G}{4\pi(1-\nu_u)} \left[\left(\frac{y(y^2-(x-2a_1)^2)}{((x-2a_1)^2+y^2)^2} - \frac{y(y^2-(x+2a_1)^2)}{((x+2a_1)^2+y^2)^2} \right) + \left(\frac{y(y^2-(x-2a_2)^2)}{((x-2a_2)^2+y^2)^2} - \frac{y(y^2-(x+2a_2)^2)}{((x+2a_2)^2+y^2)^2} \right) \right] \tag{B6}$$

$$(P_x^\lambda)^0 = -\frac{BG(1+\nu_u)}{6\pi(1-\nu_u)} \left[\left(\frac{y}{(x-2a_1)^2+y^2} - \frac{y}{(x+2a_1)^2+y^2} \right) + \left(\frac{y}{(x-2a_2)^2+y^2} - \frac{y}{(x+2a_2)^2+y^2} \right) \right] \tag{B7}$$

$$(P_y^\lambda)^0 = \frac{BG(1+\nu_u)}{6\pi(1-\nu_u)} \left[\left(\frac{(x-2a_1)}{(x-2a_1)^2+y^2} - \frac{(x+2a_1)}{(x+2a_1)^2+y^2} \right) + \left(\frac{(x-2a_2)}{(x-2a_2)^2+y^2} - \frac{(x+2a_2)}{(x+2a_2)^2+y^2} \right) \right] \tag{B8}$$

Continous of Appendix B

$$\Delta\sigma_{yy}^{ds,\lambda} = \frac{Gc(\nu_u-\nu)}{\pi(1-\nu_u)(1-\nu)} \left[\left(\frac{1}{((x-2a_1)^2+y^2)^3} - \frac{1}{((x+2a_1)^2+y^2)^3} \right) \times \left[(y(3(x-2a_1)^2-y^2)[1-(1+\xi^2)e^{-\xi^2}] - 2(x-2a_1)^2y\xi^4e^{-\xi^2}) - (y(3(x+2a_1)^2-y^2)[1-(1+\xi^2)e^{-\xi^2}] - 2(x+2a_1)^2y\xi^4e^{-\xi^2}) \right] + \left(\frac{1}{((x-2a_2)^2+y^2)^3} - \frac{1}{((x+2a_2)^2+y^2)^3} \right) \times \left[(y(3(x-2a_2)^2-y^2)[1-(1+\xi^2)e^{-\xi^2}] - 2(x-2a_2)^2y\xi^4e^{-\xi^2}) - (y(3(x+2a_2)^2-y^2)[1-(1+\xi^2)e^{-\xi^2}] - 2(x+2a_2)^2y\xi^4e^{-\xi^2}) \right] \right] \tag{B9}$$

(B10)

$$\begin{aligned}
& - \frac{2y^3\xi^4 e^{-\xi^2}}{((x-2a_1)^2 + y^2)^3} + \frac{2y^3\xi^4 e^{-\xi^2}}{((x+2a_1)^2 + y^2)^3} \\
& + \left[1 - (1 + \xi^2)e^{-\xi^2} - 2y^3\xi^4 e^{-\xi^2} \right] \frac{y(y^2 - 3(x-2a_2)^2)}{((x-2a_2)^2 + y^2)^3} - \frac{y(y^2 - 3(x+2a_2)^2)}{((x+2a_2)^2 + y^2)^3} \\
& - \left. \frac{2y^3\xi^4 e^{-\xi^2}}{((x-2a_2)^2 + y^2)^3} + \frac{2y^3\xi^4 e^{-\xi^2}}{((x+2a_2)^2 + y^2)^3} \right\}
\end{aligned}$$

$$\begin{aligned}
\Delta\sigma_{yx}^{ds,\lambda} = & \frac{Gc(v_u - \nu)}{\pi(1 - \nu_u)(1 - \nu)} \left[\left(\frac{1}{((x-2a_1)^2 + y^2)^3} - \frac{1}{((x+2a_1)^2 + y^2)^3} \right) \right. \\
& \times \left([(x-2a_1)((x-2a_1)^2 - 3y^2)[1 - (1 + \xi^2)e^{-\xi^2}] + 2(x-2a_1)y^2\xi^4 e^{-\xi^2} \right) \\
& - \left((x+2a_1)((x+2a_1)^2 - 3y^2)[1 - (1 + \xi^2)e^{-\xi^2}] + 2(x+2a_1)y^2\xi^4 e^{-\xi^2} \right) \\
& + \left(\frac{1}{((x-2a_2)^2 + y^2)^3} - \frac{1}{((x+2a_2)^2 + y^2)^3} \right) \\
& \times \left([(x-2a_2)((x-2a_2)^2 - 3y^2)[1 - (1 + \xi^2)e^{-\xi^2}] + 2(x-2a_2)y^2\xi^4 e^{-\xi^2} \right) \\
& \left. - \left((x+2a_2)((x+2a_2)^2 - 3y^2)[1 - (1 + \xi^2)e^{-\xi^2}] + 2(x+2a_2)y^2\xi^4 e^{-\xi^2} \right) \right] \quad (B_{11})
\end{aligned}$$

$$\begin{aligned}
\Delta\sigma_{xx}^{dn,\lambda} = & \frac{Gc(v_u - \nu)}{\pi(1 - \nu_u)(1 - \nu)} \left[\left(\frac{1}{((x-2a_1)^2 + y^2)^3} - \frac{1}{((x+2a_1)^2 + y^2)^3} \right) \right. \\
& \times \left([(x-2a_1)((x-2a_1)^2 - 3y^2)[1 - (1 + \xi^2)e^{-\xi^2}] + 2(x-2a_1)y^2\xi^4 e^{-\xi^2} \right) \\
& - \left((x+2a_1)((x+2a_1)^2 - 3y^2)[1 - (1 + \xi^2)e^{-\xi^2}] + 2(x+2a_1)y^2\xi^4 e^{-\xi^2} \right) \\
& + \left(\frac{1}{((x-2a_2)^2 + y^2)^3} - \frac{1}{((x+2a_2)^2 + y^2)^3} \right) \\
& \times \left([(x-2a_2)((x-2a_2)^2 - 3y^2)[1 - (1 + \xi^2)e^{-\xi^2}] + 2(x-2a_2)y^2\xi^4 e^{-\xi^2} \right) \\
& \left. - \left((x+2a_2)((x+2a_2)^2 - 3y^2)[1 - (1 + \xi^2)e^{-\xi^2}] + 2(x+2a_2)y^2\xi^4 e^{-\xi^2} \right) \right] \quad (B_{12})
\end{aligned}$$

Continuous of Appendix B

$$\begin{aligned}
\Delta\sigma_{yy}^{dn,\lambda} = & \frac{Gc(v_u - \nu)}{\pi(1 - \nu_u)(1 - \nu)} \left[\left(\frac{1}{((x-2a_1)^2 + y^2)^3} - \frac{1}{((x+2a_1)^2 + y^2)^3} \right) \right. \\
& \times \left([(x-2a_1)(3y^2 - (x-2a_1)^2)[1 - (1 + \xi^2)e^{-\xi^2}] + 2(x-2a_1)^3\xi^4 e^{-\xi^2} \right) \\
& - \left((x+2a_1)(3y^2 - (x+2a_1)^2)[1 - (1 + \xi^2)e^{-\xi^2}] + 2(x+2a_1)^3\xi^4 e^{-\xi^2} \right) \\
& + \left(\frac{1}{((x-2a_2)^2 + y^2)^3} - \frac{1}{((x+2a_2)^2 + y^2)^3} \right) \\
& \times \left([(x-2a_2)(3y^2 - (x-2a_2)^2)[1 - (1 + \xi^2)e^{-\xi^2}] + 2(x-2a_2)^3\xi^4 e^{-\xi^2} \right) \\
& \left. - \left((x+2a_2)(3y^2 - (x+2a_2)^2)[1 - (1 + \xi^2)e^{-\xi^2}] + 2(x+2a_2)^3\xi^4 e^{-\xi^2} \right) \right] \quad (B_{13})
\end{aligned}$$

$$\Delta\sigma_{yx}^{dn,\lambda} = \frac{Gc(v_u - \nu)}{\pi(1 - \nu_u)(1 - \nu)} \left[\left(\frac{1}{((x - 2a_1)^2 + y^2)^3} - \frac{1}{((x + 2a_1)^2 + y^2)^3} \right) \right. \\ \times \left[(y(3(x - 2a_1)^2 - y^2)[1 - (1 + \xi^2)e^{-\xi^2}] \right. \\ \left. - 2(x - 2a_1)^2 y \xi^4 e^{-\xi^2}) - (y(3(x + 2a_1)^2 - y^2)[1 - (1 + \xi^2)e^{-\xi^2}] \right. \\ \left. - 2(x + 2a_1)^2 y \xi^4 e^{-\xi^2}) \right] + \left(\frac{1}{((x - 2a_2)^2 + y^2)^3} - \frac{1}{((x + 2a_2)^2 + y^2)^3} \right) \\ \times \left[(y(3(x - 2a_2)^2 - y^2)[1 - (1 + \xi^2)e^{-\xi^2}] \right. \\ \left. - 2(x - 2a_2)^2 y \xi^4 e^{-\xi^2}) - (y(3(x + 2a_2)^2 - y^2)[1 - (1 + \xi^2)e^{-\xi^2}] \right. \\ \left. - 2(x + 2a_2)^2 y \xi^4 e^{-\xi^2}) \right] \left. \right] \quad (B_{14})$$

$$\Delta\sigma_{xx}^{df,\lambda} = \frac{BG(1 + \nu_u)}{6\pi(1 - \nu_u)} \left\{ \left[\sqrt{\frac{\pi}{((x - 2a_1)^2 + y^2)}} \xi \operatorname{erf} \left(\frac{(x - 2a_1)\xi}{(x - 2a_1)^2 + y^2} \right) e^{-(y^2/(x - 2a_1)^2 + y^2)\xi^2} \right. \right. \\ \left. - \frac{(x - 2a_1)}{(x - 2a_1)^2 + y^2} (1 - e^{-\xi^2}) \right. \\ \left. - \left[\sqrt{\frac{\pi}{((x + 2a_1)^2 + y^2)}} \xi \operatorname{erf} \left(\frac{(x + 2a_1)\xi}{(x + 2a_1)^2 + y^2} \right) e^{-(y^2/(x + 2a_1)^2 + y^2)\xi^2} \right. \right. \\ \left. - \frac{(x + 2a_1)}{(x + 2a_1)^2 + y^2} (1 - e^{-\xi^2}) \right] \left. \right] \\ + \left[\sqrt{\frac{\pi}{((x - 2a_2)^2 + y^2)}} \xi \operatorname{erf} \left(\frac{(x - 2a_2)\xi}{(x - 2a_2)^2 + y^2} \right) e^{-(y^2/(x - 2a_2)^2 + y^2)\xi^2} \right. \\ \left. - \frac{(x - 2a_2)}{(x - 2a_2)^2 + y^2} (1 - e^{-\xi^2}) \right. \\ \left. - \left[\sqrt{\frac{\pi}{((x + 2a_2)^2 + y^2)}} \xi \operatorname{erf} \left(\frac{(x + 2a_2)\xi}{(x + 2a_2)^2 + y^2} \right) e^{-(y^2/(x + 2a_2)^2 + y^2)\xi^2} \right. \right. \\ \left. - \frac{(x + 2a_2)}{(x + 2a_2)^2 + y^2} (1 - e^{-\xi^2}) \right] \left. \right] \left. \right\} \quad (B_{15})$$

Continuuous of Appendix B

$$\Delta\sigma_{yy}^{df,\lambda} = \frac{BG(1 + \nu_u)}{6\pi(1 - \nu_u)} (1 - e^{-\xi^2}) \left[\left[\frac{(x - 2a_2)}{(x - 2a_2)^2 + y^2} - \frac{(x + 2a_1)}{(x + 2a_1)^2 + y^2} \right] \right. \\ \left. + \left[\frac{(x - 2a_2)}{(x - 2a_2)^2 + y^2} - \frac{(x + 2a_2)}{(x + 2a_2)^2 + y^2} \right] \right] \quad (B_{16})$$

$$\Delta\sigma_{yx}^{df,\lambda} = -\frac{BG(1+\nu_u)}{6\pi(1-\nu_u)}(1-e^{-\xi^2})\left[\left[\frac{y}{(x-2a_1)^2+y^2}-\frac{y}{(x+2a_1)^2+y^2}\right]\right. \\ \left.+\left[\frac{y}{(x-2a_2)^2+y^2}-\frac{y}{(x+2a_2)^2+y^2}\right]\right] \quad (\text{B}_{17})$$

$$\Delta P_x^\lambda = -\frac{2BGc(1+\nu_u)}{3\pi(1-\nu_u)}\xi^4 e^{-\xi^2}\left[\left[\frac{y}{((x-2a_1)^2+y^2)^2}-\frac{y}{((x+2a_1)^2+y^2)^2}\right]\right. \\ \left.+\left[\frac{y}{((x-2a_2)^2+y^2)^2}-\frac{y}{((x+2a_2)^2+y^2)^2}\right]\right] \quad (\text{B}_{18})$$

$$\Delta P_y^\lambda = -\frac{2BGc(1+\nu_u)}{3\pi(1-\nu_u)}\xi^4 e^{-\xi^2}\left[\left[\frac{(x-2a_1)}{((x-2a_1)^2+y^2)^2}-\frac{(x+2a_1)}{((x+2a_1)^2+y^2)^2}\right]\right. \\ \left.+\left[\frac{(x-2a_2)}{((x-2a_2)^2+y^2)^2}-\frac{(x+2a_2)}{((x+2a_2)^2+y^2)^2}\right]\right] \quad (\text{B}_{19})$$

$$\Delta P_f^\lambda = \frac{B^2G(1-\nu)(1+\nu_u)^2}{9\pi(1-\nu_u)(\nu_u-\nu)}\left\{\left[\left[\sqrt{\frac{\pi}{2((x-2a_1)^2+y^2)}}\xi \operatorname{erf}\left(\frac{(x-2a_1)\xi}{(x-2a_1)^2+y^2}\right)e^{-(y^2/(x-2a_1)^2+y^2)\xi^2}\right]\right. \right. \\ \left. - \left[\sqrt{\frac{\pi}{2((x+2a_1)^2+y^2)}}\xi \operatorname{erf}\left(\frac{(x+2a_1)\xi}{(x+2a_1)^2+y^2}\right)e^{-(y^2/(x+2a_1)^2+y^2)\xi^2}\right]\right] \\ \left. + \left[\left[\sqrt{\frac{\pi}{2((x-2a_2)^2+y^2)}}\xi \operatorname{erf}\left(\frac{(x-2a_2)\xi}{(x-2a_2)^2+y^2}\right)e^{-(y^2/(x-2a_2)^2+y^2)\xi^2}\right]\right. \right. \\ \left. - \left[\sqrt{\frac{\pi}{2((x+2a_2)^2+y^2)}}\xi \operatorname{erf}\left(\frac{(x+2a_2)\xi}{(x+2a_2)^2+y^2}\right)e^{-(y^2/(x+2a_2)^2+y^2)\xi^2}\right]\right] \right\} \quad (\text{B}_{20})$$

$$\text{and } \xi = \sqrt{\frac{r^2}{4ct}}$$

شبیه سازی مکانیسم انتشار ترک در محیط متخلخل با استفاده از روش توسعه یافته ناپیوستگی جابجایی المان خطی

محمد حسین دهقانی فیروزآبادی^۱، محمد فاتحی مرجی^{۱*}، ابوالفضل عبدالهی پور^۲، علیرضا یار احمدی بافقی^۱، و یوسف میرزائیان^۱

۱-دانشکده مهندسی معدن و متالورژی، دانشگاه یزد، یزد، ایران

۲-دانشکده مهندسی معدن، دانشگاه تهران، تهران، ایران

ارسال ۲۰۲۲/۰۹/۰۲، پذیرش ۲۰۲۲/۰۹/۳۰

*نویسنده مسئول مکاتبات: mohammad.fatchi@gmail.com

چکیده:

کاربری زمین (LU) یکی از ضروری‌ترین بخش‌های اطلاعات نقشه برداری است که برای نظارت بر محیط معدن استفاده می‌شود. استخراج مجموعه داده‌های کاربری زمین از تصاویر ماهواره‌ای سنجش از راه دور، توجه قابل توجهی را در جامعه منطقه معدنی به خود جلب کرده است. با این حال، طبقه‌بندی LUs از تصاویر ماهواره‌ای به دلیل در دسترس نبودن مجموعه داده‌های مرتبط با استخراج زغال‌سنگ کارآمد، یک کار خسته‌کننده است. روش‌های یادگیری عمیق اهرم بزرگی برای استخراج اطلاعات معنی‌دار از تصاویر ماهواره‌ای با وضوح بالا فراهم می‌کند. علاوه بر این، عملکرد یک رویکرد طبقه بندی یادگیری عمیق به طور قابل توجهی به کیفیت مجموعه داده‌ها بستگی دارد. کار حاضر تلاش می‌کند تا تولید مجموعه‌های داده مبتنی بر ماهواره را برای تحلیل عملکرد الگوریتم‌های یادگیری مبتنی بر شبکه‌های عصبی عمیق (DNN) در طبقه‌بندی‌های LU مناطق معدنی نشان دهد. مناطق معدن به طور کلی بر اساس بازرسی بصری به مناطق مجزایی زمین‌های بایر، مناطق ساخت و ساز شده، بدنه آبی، پوشش گیاهی و معادن زغال سنگ فعال طبقه بندی می‌شوند. در کار تجربی ما، یک روش و راه از ۱۰۰ نمونه فضایی برای هر یک از پنج ویژگی در سه مقیاس، به عنوان $[۳ \times ۱ \times ۱]$ ، $[۳ \times ۵ \times ۵]$ و $[۳ \times ۱۰ \times ۱۰]$ تولید می‌شود. علاوه بر این، اثرات مقیاس پذیری‌های مختلف مجموعه داده بر عملکرد طبقه بندی نیز تجزیه و تحلیل می‌شود. همچنین این مطالعه موردی برای معیار مقیاس بزرگ مجموعه داده‌های تصاویر ماهواره‌ای برای مناطق معدنی اجرا شده است. در آینده، این کار می‌تواند برای طبقه بندی LU در مناطق مورد مطالعه مربوطه در زمان واقعی استفاده شود.

کلمات کلیدی: روش ناپیوستگی جابجایی، المان‌های مرتبه بالا، پوروالاستیک، راه حل‌های اساسی، انتشار ترک، مکانیک شکست سنگ.